

# **OFFSHORE PIPELINE LEAK MODELING USING A COMPUTATIONAL FLUID DYNAMICS APPROACH**

By

© Yousef Abdulhafed Yousef

A thesis submitted to the  
**School of Graduate Studies**  
in partial fulfillment of the requirements for the degree of  
**Master of Engineering**

**Faculty of Engineering and Applied Science**  
**Memorial University of Newfoundland**

**Oct 2018**

St. John's

Newfoundland

## **Abstract**

Pipelines laid over long distances in the harsh offshore environment may be affected by excessive straining, corrosion, scouring, iceberg and other third-party damages. Small chronic leaks may cause severe safety and environmental effects if left undetected for a long time. A CFD model of a subsea leaking pipeline is developed to predict the pressure and temperature profiles around the pipe's leak surroundings. The developed CFD model is used to study a pipeline section with a leak on the top. It considers the fluid inside the pipeline as well as the fluid surrounding the pipeline and does a combined simulation of the system. In addition, a hydrodynamic model is used to evaluate the parameters of a full-scale 150 km long-distance pipeline. This hydrodynamic model is developed to find the most critical section of the proposed long pipeline system. Furthermore, the hydrodynamic model provides the boundary conditions for the CFD model. The developed model was used to perform parametric studies to understand the impact of leaks on the surrounding water. The present study will help pipeline operators to select the most appropriate leak detection technology with the right specifications for the pipeline systems; especially to optimize Fiber Optic Cable (FOC) based Distributed Temperature Sensing (DTS) Solutions.

## **Acknowledgments**

First, all praise is to God by whose grace good deeds are completed. After, I would like to express my profound gratitude to my supervisors Professor Syed Imtiaz and Professor Faisal Khan for their patient guidance, understanding and excellent advice during the course of this work. Their motivation and full support have not only made the completion of this thesis possible but has left an impression that will continue to influence my work. I also acknowledge the financial support provided by the Natural Sciences and Engineering Research Council (NSERC) of Canada, Canada Research Chair (Tier I) program.

My sincere appreciation and special thanks to my mother, my wife, my children and my brothers and sisters for their love, support, prayers and for patiently enduring many sacrifices as a result of this dissertation.

Last, but not least, I'm thankful to Professor Amer Aborig and Mr. Christopher Penny for being helpful in some of my research struggles as well as all my close friends for their encouragement to pursue this degree.

# Table of Contents

Abstract.....	II
Acknowledgments.....	III
Table of Contents.....	IV
List of Tables .....	VIII
List of Figures.....	IX
Nomenclature.....	XI
Abbreviations.....	XIII
CHAPTER 1: INTRODUCTION.....	1
1.1 Overview.....	1
1.1.1 Overview of leak detection systems.....	2
1.1.2 Overview of Computational Fluid Dynamics.....	6
1.2 Problem Statement.....	8
1.3 Contributions.....	10
1.4 Objectives of the Research.....	11
1.5 Thesis Outline.....	12
CHAPTER 2: REVIEW OF LITERATURE.....	14

2.1	Preface.....	14
2.2	Conventional Leak Detection Systems .....	14
2.3	Pipeline Leakage modeling using CFD approach.....	25
CHAPTER 3: THEORY AND GOVERNING EQUATIONS.....		29
3.1	Overview .....	29
3.2	Review of Theory .....	29
3.3	Hydrodynamic model governing equations .....	33
3.3.1	Steady-state in the hydrodynamic model.....	35
3.3.2	Transient flow in the hydrodynamic model.....	37
3.4	CFD Model governing equations.....	40
3.4.1	Pre-analysis.....	40
3.4.2	CFD k- $\epsilon$ turbulence model.....	40
3.4.3	Computational details.....	42
3.5	Summary .....	43
CHAPTER 4: OFFSHORE PIPELINES HYDRODYNAMIC SIMULATION .....		44
4.1	Overview .....	44
4.2	Methodology of the Hydrodynamic Simulation .....	44
4.3	Applications of the Methodology .....	46

4.4	Simulation Results .....	49
4.4.1	Boundary Condition Assessment by Hydrodynamic Model .....	49
CHAPTER 5: PIPELINE LEAKAGE COMPUTATIONAL FLUID DYNAMICS		
SIMULATION.....		
		52
5.1	Overview .....	52
5.2	Methodology of the CFD Simulation .....	52
5.3	Application of the Methodology .....	54
5.4	CFD Simulation Result .....	58
5.4.1	Model Validation .....	58
5.4.2	Transient Simulation for Leak Behaviour Characterization.....	60
5.4.3	Volume of Fraction Effect on Temperature Profiles .....	63
5.4.4	Leak Size Sensitivity Analysis on Temperature Profiles .....	64
CHAPTER 6: CONCLUSIONS AND RECOMMENDATIONS.....		
		72
6.1	Conclusions.....	72
6.2	Recommendations.....	74
6.3	Future work .....	75
Bibliography .....		76
Appendices.....		84

Appendix A: AFT Model’s Data .....	84
I. Single-Phase Flow Case .....	84
I.1 <i>Input data single-phase flow case:</i> .....	84
I.2 <i>Output data single-phase flow case:</i> .....	85
II. Multi-Phase Flow Case .....	86
II.1 <i>Input data multi-phase flow case:</i> .....	86
II.2 <i>Output data multi-phase flow case:</i> .....	87
Appendix B: CFD Model’s Output Data .....	88
I. Pressure Profile .....	88
I.1 <i>Pressure profile at different leak sizes for Single-phase flow case:</i> .....	88
I.2 <i>Pressure profile at different leak sizes for Multi-phase flow case:</i> .....	88
II. Temperature Profile .....	89
II.1 <i>Temperature profile at different leak sizes for Single-phase flow case:</i> .....	89
II.2 <i>Temperature profile for multi-phase flow case</i> .....	90
III. Mass flow rate and velocity profiles .....	90
III.1 <i>Mass flow rate at different leak sizes</i> .....	90
III.1 <i>3D Condensate velocity profile Vs time</i> .....	91
III.1 <i>Cont. 3D Condensate velocity profile Vs time</i> .....	92
III.1 <i>Condensate pressure profile Vs Time</i> .....	93

## List of Tables

Table 3-1: Condensate compositions mole fraction.....	38
Table 4-1: Input fluid properties and initial boundary condition for hydrodynamic model.....	47
Table 4-2: Condensate compositions (mole fraction), after Saleh and Stewart [59] .....	48
Table 4-3: Fluid properties and critical segment information .....	51
Table 5-1: Boundary conditions and the fluid parameters for the CFD STAR-CCM simulation model .....	56
Table 5-2: The volume of fraction (VOF) for gas condensate composition.....	57
Table 5-3: Volume of fraction (VOF) of vapour and liquid phases, for condensates (1, 2, and 3) .....	63

## List of Figures

Figure 2-1: A schismatic view of the CFD procedure (after Wilcox) [11].....	8
Figure 4-1: Pressure drop along pipeline with and without leak (after Dinis, 1998).....	29
Figure 5-1: Procedures of hydrodynamic simulation by steps to study the pipeline leak and its impact on seawater .....	46
Figure 5-2: Hydrodynamic physical model components .....	46
Figure 5-3: Pipeline pressure profiles of the hydrodynamic model in single-phase and multi- phase flow .....	49
Figure 5-4: Fluid flow velocity profiles of the hydrodynamic model for single-phase and multi- phase flows .....	50
Figure 5-5: Pipeline fluid temperature profiles of the hydrodynamic model for single-phase and multi-phase flows .....	50
Figure 6-1: Procedures by steps to study the pipeline leak and its impact on sea water .....	54
Figure 6-2: Pipeline physical model and leak position.....	55
Figure 6-3: Isometric view of pipeline geometry for CFD model using STAR-CCM software ..	55
Figure 6-4: Refined meshing of pipeline at the near wall and leak hole .....	57
Figure 6-5: CFD model validation with Ben-Mansour’s work (pipe length 2 m, leak sizes 2mm &10 mm, velocity 1 m/s, pressure 1 bar) [36].....	59
Figure 6-6: CFD model validation of temperature changes $\Delta T$ with leak sizes increase, compared with experimental jet-plume thermal gradient for liquid leaks, by Siebenaler et al. [40].....	60
Figure 6-7: Pressure profile for single-phase flow case, along the pipe’s outer wall for leak sizes from 2 to 14 mm at 0.5 m from inlet .....	62

Figure 6-8: Pressure profile for multi-phase flow case, along the pipe’s outer wall for leak sizes from 2 to 14 mm at 0.5 m from inlet .....	63
Figure 6-9: Temperature Profile for Condensates 1, 2 and 3, along the pipe’s outer surface with 2 mm leak size .....	64
Figure 6-10: Temperature profiles for single phase flow case, along the pipe’s outer surface for leak sizes from 0 to 14 mm at 0.5 m distance from the pipe inlet .....	65
Figure 6-11: Temperature profiles for multi-phase flow case, along the pipe’s outer surface for leak sizes from 2 to 14 mm at 0.5 m distance from the pipe inlet .....	66
Figure 6-12: Temperature contours around the leak in single-phase flow for leak sizes from 2 to 8 mm at 0.5 m from inlet .....	67
Figure 6-13: Temperature contours around the leak in multi-phase flow for leak sizes from 2 to 14 mm at 0.5 m from inlet .....	67
Figure 6-14: Sensitivity chart of leak size effect on $\Delta T$ for single-phase flow at 0.5 m from inlet .....	68
Figure 6-15: Sensitivity chart of leak size effect on $\Delta T$ for multi-phase flow at 0.5 m from inlet .....	69
Figure 6-16: Temperature vertical range on top of pipe leak for single-phase flow .....	70
Figure 6-17: Temperature vertical range on top of pipe leak for multi-phase flow .....	70

## Nomenclature

<b>Symbol</b>	<b>Definition</b>
$A$	Cross-section area of the pipe ( $\text{m}^2$ )
$C_{pro}$	Proportionality constant
$C_{sp}$	Pressure coefficient
$c_p$	Specific heat at constant pressure ( $\text{J/kg K}$ )
$c_v$	Specific heat at constant volume ( $\text{J/kg K}$ )
$D$	Pipe diameter (m)
$e$	Roughness coefficient (–)
$f$	Friction factor (–)
$F$	Fanning friction coefficient (–)
$g$	Net body force per unit mass (the acceleration of gravity) ( $\text{m/s}^2$ )
$k$	Von Karman constant
$k_L$	Heat transfer coefficient ( $\text{W/m K}$ )
$L$	Pipeline length (m)
$M$	Mass flow ( $\text{kg/s}$ )
$P$	Pressure (Pa)
$p(x)$	Pressure at $x$ (Pa)
$q$	Heat addition per unit mass per unit time ( $\text{W/kg}$ )
$Re$	Reynolds number (–)
$R$	Specific gas constant ( $\text{J/kg K}$ )
$t$	Time (s)

$T$	Temperature
$T_{\text{gas}}$	Gas Temperature (K)
$T_{\text{Amb}}$	Ambient temperature (K)
$v$	Mean velocity (m/s)
$V$	Flow velocity (m/s)
$x$	Spatial coordinate (m)
$Z$	Compressibility factor (-)

## Abbreviations

Symbol	Definition
LDS	Leak Detection Systems
CFD	Computational Fluid Dynamics
DTS	Distributed Temperature Sensing
FOC	Fiber Optic Cable
AFT	An Applied Flow Technology application
STAR-CCM	A CFD application
ANSYS FLUENT	A CFD application
COMSOL	A CFD application

## Greek symbols

$\alpha$  Angle between the horizon and the direction x

$\Phi$  Thermal conductivity coefficient of the fluid

$\mu$  Viscosity of fluid ( $\text{N s/m}^2$ )

$\rho$  Density ( $\text{kg/m}^3$ )

$\epsilon$  Roughness of the inner pipe surface (–)

$\varepsilon$  Turbulent dissipation, [ $\text{m}^2\text{s}^{-3}$ ]

$\tau$  Shear stress, [ $\text{Nm}^2$ ]

$\delta$  Delta function

$\lambda$  Thermal conductivity coefficient of gas ( $\text{W/m K}$ )

## Quantities

$C_\mu, C_{\varepsilon 1}, C_{\varepsilon 2}, C_S, \rho_k, \rho_\varepsilon$  Model constant parameters for k- $\varepsilon$

$\mu_t$  Turbulent viscosity (Ns/m<sup>2</sup>)

$\sigma$  Prandtl number

$u, v, w$  Filtered velocity field

$x$  Spatial coordinate (m)

## **Chapter 1: Introduction**

### **1.1 Overview**

With the growing global dependence on hydrocarbon products, it is very important to ensure the continuity of new hydrocarbons discovery. Also, it is very important to ensure that the hydrocarbons are extracted in an environmentally sustainable manner, and the produced quantities are efficiently delivered by assuring their safe transportation and distribution from the place of production to place of consumption. Pipeline transport system is a unique form of transportation that involves the transportation of fluids through pipes, getting a wide range of utilization in the oil and gas industry. Pipelines can range from few meters to few thousand kilometers, in the United States for example, there are total pipeline length of about 793,285 km, Russia about 231,000 km, Canada about 98,544 km, United Kingdom about 29,167 km, while Nigeria has about 11,647 km [1]. Leaks are among the major threats to pipeline transport systems, which could be due to installation defects, corrosion, anchor snagging dropped object, vessel grounding and mechanical impact. The occurrence of leaks in pipeline systems does not only signify a loss of valuable, hydrocarbon resource but also a source of environmental pollution and potential of disasters. The recent increase in the utilization of pipeline systems for oil and gas transportation together with the great economic loss and environmental implication associated with their failure calls for a need to explore cheap, quick, accurate and reliable leak detection methods in pipeline systems using real-time monitoring technologies.

### **1.1.1 Overview of leak detection systems**

The most common way of categorizing leak detection systems (LDS) is based on their technical nature [2]. LDSs are categorized into two main classes: hardware-based methods and software-based methods. These two classes are sometimes mentioned as externally or internally based LDSs. Hardware-based methods depend on mainly the usage of special sensing devices in the detection of fluid leaks. The hardware-based systems detect the leaks from outside of the pipe using specific sensing devices. These hardware systems can be further classified as optical, acoustic, cable sensor, soil monitoring, ultrasonic flow meters and vapour sampling. The software-based systems have analytical methods at their core. The applied algorithms continuously monitor the state of temperature, pressure, flow rate or other pipeline parameters and can infer, based on the evolution of these quantities, if a leak has occurred. The software systems can use different approaches to detect leaks: mass/volume balance, acoustic/negative pressure wave, real-time transient modeling, pressure point analysis, statistics or digital signal processing [3]. The software-based systems may require flow, pressure and temperature measurements at the inlet and outlet. Internal-based systems use field sensor data that monitors internal pipeline parameters, such as pressure, temperature, viscosity, flow rate, density, contamination, product sonic velocity and product data at interface locations. These inputs are then used for inferring a release/leak of fluid by computation. Typically, these systems are installed along with the pipeline and other data acquisition systems. These calculation based technologies usually have a considerable track record for detecting large and some small pipeline leaks. However, further technology

advancements are essential in response to the demands from pipeline operators, regulators and the public for safety and environmental improvements. In special cases, pipeline projects have been deployed with advanced LDSs to help improve the ability to detect small, chronic leaks below the detection threshold of conventional LDS technologies. The pipeline industry is advancing in many of the offshore areas, which makes conventional remote sensing of small leaks more challenging. Thus, external LDS technologies are essential for detecting small, chronic leaks. External LDS can quickly sense and locate small leaks and provide the required information for risk mitigation. They can detect leaks below the minimum thresholds of detection of internal LDS. Depending on the technology, some external LDS still have certain limitations and being not very sensitive to smaller leaks. FOC distributed sensors technology is one of the most advanced LDS that can detect and locate small leaks precisely. LDSs such as Distributed Temperature Sensing (DTS) technology can accurately detect the location of small chronic leaks by sensing local temperature changes [4]. It works by sensing minute changes in the temperature surrounding the pipeline due to leaks and can locate tiny leaks precisely [5], [6]. Thus FOC distributed sensing technology is becoming a significant monitoring system for other industries but it has had limited use to date for monitoring potential leakage.

Fibre Optic Leak Detection Systems are much appropriate to a wide range of single and multiphase liquids and gases including ammonia, ethylene, natural gas and heavy oil as well as cryogenic mediums such as LNG, LPG, etc. Such applications can similarly be offshore as well as onshore. Fiber optic technologies rely on the installation of a fiber

optic cable all along the pipeline. The cable acts as a continuous, distributed sensor along the length of a pipeline. The leakage can be detected by monitoring the temperature changes history in the fiber optic cable system. Optical sensing has highlighted much attention in related industries. The pipeline physical parameters can be measured via processing optical signals that spread along the fibers. Fiber optic sensors have remarkable advantages such as high precision, electromagnetic interference immunity, high sensitivity corrosion resistance and high reliability. It is noticeable that fiber optic sensors have overcome many conventional difficulties and provide accurate and steady pipeline monitoring [5], [7].

There are three distributed fiber optic technologies that are available for monitoring a pipeline: Distributed Temperature Sensing (DTS). Distributed Temperature Sensing (DTS) is one of the most effective solutions based on Fiber Optic Cable (FOC) technology. FOC itself works as the sensor and data link for the DTS solution. Oil leakage leads to a local temperature increase, but gas leakage will lead to local cooling. DTS uses a temperature analyzing instrument to measure temperature. There are two backscattered light bands that respond to temperature and are available for DTS monitoring. One is Raman, and the other is Brillouin. Light in the Raman band reacts to temperature variations by an increase or decrease in intensity. Light in the Brillouin band reacts to temperature variations by a shift in wavelength. While both bands have been used by different vendors positively for different applications, Brillouin based DTS systems are more engaging than Raman based DTS systems for long-distance pipeline

leak detection [4], [6]. The technology is effectively utilized for fire detection in constructions, for which a fire will cause significant temperature changes ( $\Delta T$ ).

Nevertheless, for pipeline leak detection, temperature changes might be insignificant to detect chronic leaks. A temperature change caused by a leak must rise or drop the normal operating temperature of the DTS system's fixed fiber optic cable that is installed within the water surrounding a pipeline above the DTS temperature sensitivity [6], [7]. DTS systems are optoelectronic devices which measure temperatures by means of optical fibers functioning as linear sensors. Temperatures are logged along the optical sensor cable, thus not at points, but as a continuous profile. A high accuracy of temperature determination is attained over great distances. Generally, the DTS systems can trace the temperature to a spatial resolution of 1 m with accuracy to within  $\pm 1^\circ\text{C}$  at a resolution of  $0.01^\circ\text{C}$  [7]. Knowing the significance of LDSs in the prevention of oil spills and the need for a more detailed understanding of the use and effectiveness of leak detection technologies has led key oil companies to adopt the best possible technologies available. It is difficult for a pipeline company to distinguish, what is the best solution for their particular pipeline and philosophy of operation without a deep understanding of the leak's behaviour. Thus, subsea pipeline leaks modeling using CFD will assist pipeline operators to establish specifications for Fiber Optic Cable Distributed Sensing Solutions. A fast leak detection technique like DTS is very important to mitigate environmental and economic impacts.

### **1.1.2 Overview of Computational Fluid Dynamics**

A key element of assessing the applicability of LDSs is to characterize the behaviour of leaks. It is critically important to understand how leaks behave when employing a technology that has only been previously used for other conditions. Computational fluid dynamics or CFD is the representation of systems involving fluid flow, heat transfer and related phenomena like chemical reactions by means of computer-based simulation. The technique is very powerful and extends a wide range of industrial and non-industrial use areas. The key solution to a flow problem (velocity, pressure, temperature etc.) is defined at nodes inside each cell. The precision of a CFD solution is governed by the number of cells in the grid. Both the precision of a solution and its cost in terms of essential computer hardware and calculation time are dependent on the refinement of the grid. Best meshes are often non-uniform: finer in areas where large discrepancies occur from point to point and coarser in areas with relatively slight change. It is still up to the skills of the CFD user to improve the grid that is a suitable compromise between desired precision and solution cost. [8], [9]. The finite volume method is more common for the most well-established CFD codes like STAR-CCM [8], [10]. In a framework of numerical algorithm consists of the following steps:

1. Integration of the governing equations of fluid flow over all the (finite) control volumes
2. Discretization is the transformation of the resulting integral equations into a system of algebraic equations
3. Solution of the algebraic equations by an iterative method

The working principle of CFD is built on three elements; the pre-processor, solver and post-processor as follows:

- 1- Pre-processor:** Pre-processor includes the input of the flow problem to a CFD program by means of an operator-friendly interface and the subsequent conversion of this input into a form appropriate for use by the solver. The region of fluid to be analyzed is called the computational domain and it is made up a number of discrete elements that called the mesh (or grid).
- 2- Solver:** Solver computes the solution of the CFD problem by solving the governing equations. The equations governing the fluid motion are Partial Differential Equations (PDE) made up of combinations of flow variables (e.g. velocity and pressure) and derivatives of these variables. The PDE's are converted into algebraic equations [11]. This process is known as numerical discretization. There are four methods for it; (i) Finite difference (ii) Finite element method (iii) Finite volume method and (iv) Spectral method. The finite difference and finite volume method both produce solutions to the numerical equations at a given point depends on the values of the neighboring points, whereas the finite element produces equations for each element individually of all other elements. In the current work STAR-CCM which is based on finite volume method is used for the simulation.

**3- Post-processor:** It is used to visualize and quantitatively process the results from the solver part. In a CFD package, the analyzed flow phenomena can be displayed in vector plots or contour plots to display the trends of velocity, pressure, kinetic energy and other properties of the flow.

The following figure shows a schematic view of the CFD procedure:

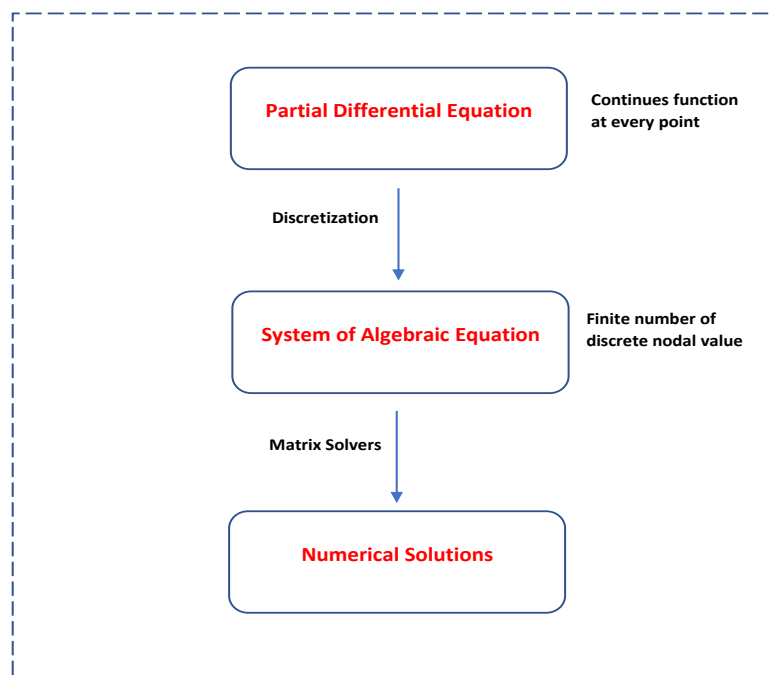


Figure 1-1: A schismatic view of the CFD procedure (after Wilcox) [11].

## 1.2 Problem Statement

Hydrocarbon transport through subsea pipelines is a cost-effective and reliable way of distribution. Offshore pipelines' leakage problems must be minimized. Leak Detection Systems (LDSs) have been in use for a long time to help in pipeline monitoring. Offshore pipelines' monitoring poses more challenges because of the remoteness, long-distance

installations and the need of power. Any potential offshore subsurface leaked hydrocarbon may not be detected for a long time and could lose a considerable hydrocarbon volume under the sea's winter ice cover. Prior publications have classified LDSs into the Non-software type, externally based systems or Software type, internally based systems [2]-[4], [12], [13]. Most of those LDSs are not suitable for offshore operations because of the remote maintenance challenges, long-distance installations and the need for power. It is hard for a pipeline operator to distinguish, what is the best solution for their particular pipeline and philosophy of operation without a deep understanding of the leak's behaviour. Advanced LDS can accurately recognize the location of small chronic leaks by detecting local temperature changes, longitudinal strains and vibrations [4]. For example, FOC technologies can sense and locate tiny leaks precisely as well as minimize false alarms [5], [6]. FOC based DTS technology is one of the reliable advanced LDS because of its capability of detecting the location of small chronic leaks precisely. It works by sensing minute changes in the temperature surrounding the pipeline due to leaks. In order to design an effective DTS, there is a need to understand and collect some accurate information about the leak's behaviour and its environmental implications. However, it has not been extensively studied in terms of CFD simulations of the leak's effects on the surroundings. Hence, this study proposed pipeline leaks simulations using CFD approach that will assist pipeline operators to design the optimal LDS for their pipeline system.

### **1.3 Contributions**

The main purpose of this study is to understand a leak's effect on the water surrounding and the pipeline outer wall. The unique approach of this study is to simulate the fluid flow from inside the pipeline leaking into the unsteady ocean water in one computational environment. Furthermore, this model will examine the leak size effect on the temperature and pressure profiles. The available CFD modeling software packages are intended to model a small pipeline section, due to limitations caused by cost and runtime. Hence, the CFD model is augmented by a hydrodynamic model to evaluate the conditions of the entire pipeline. The hydrodynamic model of 150 km pipeline length has been established using AFT software to examine the temperature and pressure profiles along the entire distance. The most critical segment is then suggested for a sophisticated CFD simulation based on the most extreme condition, among the 150 km of the pipeline. The hydrodynamic model provided the initial required parameters and boundary conditions for the CFD simulations. A CFD model of a pipeline section with a leak in the top is developed to predict the pressure and temperature profiles around the pipe's leak surroundings. Further, single-phase and multi-phase flow simulations are conducted to observe the local pressure and temperature changes for different leak sizes. The effect of VOF variation in multi-phase flow is also been examined. Moreover, the effect of different leak sizes on temperature sensitivity around the leak hole has been studied. Sensitivity analyses of the temperature and leak sizes for both single-phase and multi-phase flow have been presented.

The developed simulations in this study provided helpful outcomes that can help pipeline operators to understand the pipeline leakage behaviour under the sea water.

#### **1.4 Objectives of the Research**

Offshore pipelines' leakage problems must be minimized. Leak Detection Systems (LDSs) have been in use for a long time to help in pipeline monitoring. Offshore pipelines' monitoring poses more challenges because of the remoteness, long-distance installations and the need of power. LDSs such as Distributed Temperature Sensing (DTS) technology can accurately detect the location of small chronic leaks by sensing local temperature changes. It is difficult for a pipeline company to distinguish, what is the best solution for their particular pipeline without a deep understanding of the leak's behaviour. Hence, there is a need to understand and collect some accurate information about the leak's effect on the surrounding environment. Therefore, the aim of this study is to understand a leak's effect on the surrounding water and the pipeline's outer wall by using the CFD approach. This study proposed a methodology that can be used by pipeline operators to exactly determine the specifications for the DTS based leak detection technologies.

## **1.5 Thesis Outline**

The traditional format was adopted to write this thesis. An outline of each chapter is provided as follows:

Chapter one briefly introduces the pipeline transport system, leak detection systems, and the CFD concepts. It also describes the problem and the research contributions and objectives.

Chapter two gives the literature review covering the conventional leak detection systems and the more recent analytical and numerical approaches.

Chapter three discusses the theoretical background of basic equations that describe fluid motion in leaked pipelines. Also, it simplifies how CFD formulates these equations. By using those equations, the Navier-Stokes equations are presented. It also gives the characterizations of turbulence for the hydrodynamic and CFD models.

In chapter four, a hydrodynamic simulation is presented as the first stage in the overall methodology. The organization of the simulation methodology is presented. Also, the application of the methodology was demonstrated. In the end, results of the simulation are presented and discussed.

In chapter five, a CFD model is presented. Also, a detailed diagram of the simulation steps is presented as a second stage in the overall methodology. Application of the methodology was illustrated. The model validations were verified with two previous works. Results of the simulations were discussed and compared with previous findings.

The various parameters such as velocity, temperature and pressure profiles have been investigated with each turbulence model for single-phase and multi-phase flow. The volume of Fraction effect on the temperature changes was also examined. Last, sensitivity analyses of the temperature and leak sizes for both single-phase and multi-phase flow were presented.

Chapter six focuses mainly on the conclusions, recommendations and suggestions for further studies.

Finally, the list of references is arranged using RefWorks tool and displayed with IEEE format in order by number and the Appendices that presented the model's input and output data are attached.

## **Chapter 2: Review of Literature**

### **2.1 Preface**

The purpose of this study is to investigate subsea pipeline leaks and their impact on the surroundings. Traditional methods to detect subsea pipeline leaks are based on internal flow condition measurements (e.g. internal pressure, flow rate, mass/volume balance), which are good for detecting large and maybe some small pipeline leakage in normal environmental condition. Offshore pipelines require special and improved systems to be able to detect very small chronic leaks. Advanced hardware-based methods can detect the presence of leaks from outside the pipeline by using suitable equipment. These kinds of techniques are featured by a significant sensitivity to leaks and are very precise in finding the leak location. However, the installation of their equipment is very expensive and complicated. Examples of this method are acoustic leak detection, fiber optical sensing cable, vapour sensing cable and liquid sensing cable-based systems. A literature survey has been performed to review the various conventional, experimental and numerical techniques used for leak detection. The present study focuses on numerical modeling of the subsea pipeline leakages to fill the research gap.

### **2.2 Review of Leak Detection Systems Classifications**

The various commercially available leak detection systems can be classified as either internal-type leak detection systems or external-type leak detection systems. Some require periodic survey inspections of the pipelines such as periodic pig runs with an acoustic sensing tool. Others are more suited for onshore applications. The following

section is a brief review of the technologies that can be permanently installed with the pipelines and are considered suitable for offshore leak detection applications.

### **I- Internal Leak Detection Systems**

- Mass Balance with Line Pack Compensation.
- Pressure Trend Monitoring.
- Real Time Transient Monitoring.
- Pressure Safety Low (PSL).
- Periodic Shut-In Pressure Tests.
- Pressure Wave / Acoustic Wave Monitoring

### **II- External Leak Detection Systems**

- Vacuum Annulus Monitoring.
- Hydrocarbon vapour Sensing Systems.
- Distributed Temperature Sensing (DTS) Fiber Optic Cable Systems.
- Distributed Acoustic Sensing (DAS) Fiber Optic Cable Systems.
- Distributed Strain Sensing (DSS) Fiber Optic Cable Monitoring Systems (not necessarily a leak detection system)

### **2.2.1 Internal Leak Detection Systems**

Internal leak detection systems rely on internal pressure, temperature, flow rate, and/or density measurements [5, 6, 14 &18]. They are sometimes referred to as computational leak detection systems. However, there are also external leak detection systems that rely on computations to monitor pipelines for leaks.

#### **2.2.1.1 Mass Balance with Line Pack Compensation (MBLPC)**

MBLPC is an accounting technique that compares the flow entering a pipeline system to the flow leaving a pipeline system. The flow rates are adjusted for temperature and pressure measurements at the inlet flow meter, outlet flow meter, and any flow meters in between. This type of system works well and can achieve leak detection thresholds that are less than 1% of flow within single phase pipelines, especially if daily accounting over multiple days is made [6]. The system does not provide as low of a minimum leak detection threshold limit capability for multi-phase pipelines as it does on single phase pipelines. Multi-phase meters have worse flow measurement accuracies than most single phase flow meters, and multi-phase pipelines have greater variations of liquid hold-up. Pressure trend monitoring or real time transient analysis monitoring may provide better leak detection threshold limits for multi-phase pipelines [6 &18].

#### **2.2.1.2 Pressure Trend Monitoring**

Pressure trend monitoring uses pressure measurements to screen operating trends in the pipeline. If a set of parameters does not match historical trends, an alarm is triggered. Pressure trend monitoring systems tend to catch larger leaks faster than MBLPC on

single phase liquid pipelines, but pressure trend monitoring systems may have worse leak detection threshold limits than MBLPC systems for single phase pipelines [6].

### **2.2.1.3 Real Time Transient Monitoring**

Real time transient monitoring includes analyzing flow conditions based on flow rate, pressure, and temperature data acquired from instruments and meters to estimate flow conditions along the pipeline. These estimates are performed on a real-time basis and are compared to the flow rate, pressure, and temperature measurements at the various instruments and meters. If estimates differ enough from real measurements, then an alarm is triggered. These systems are still prone to precision limitations of instruments, and there is a limiting leak detection threshold. Real time transient monitoring may be a good choice for multi-phase pipelines [6].

### **2.2.1.4 Pressure Safety Low**

Pressure safety low (PSL) monitoring is one of the more shared leak detection monitoring methods employed on non-arctic pipeline projects. Although a formal leak detection software system is not part of the system, logic controllers linked to pressure transmitters are used. Pressure alarm settings are set below the normal operating pressure ranges that happen at locations where a pressure transmitter is acquiring pressure measurements (i.e. near the inlet and outlet of a pipeline). A large enough leak may cause the pressure at the inlet and/or outlet of the pipeline to fall below the normal operating pressure limit and the low pressure alarm setting, thereby triggering an alarm that a leak may have occurred.

A leak must be large enough to drop the pressure at one or more of the pressure transmitters in the pipeline below the PSL alarm setting. Typically, large leaks have been noticed with PSL systems, and very small leaks have gone undetected until sheens on the water surface were visually seen during over-flights of the pipeline routes [6].

#### **2.2.1.5 Periodic Shut-In Pressure Tests**

Periodic shut-in pressure tests are sensitive tests that can have a leak detection threshold that approaches zero. It may detect all leaks, including chronic leaks. It can be used for pipelines that have periodic batch flows where the flow requirements allows periodic shut-down of the pipeline over a period of time that can support shut-in pressure tests. However, pipeline shut-downs are not compatible with most oil and gas applications, and this is especially true for deep-water and cold areas developments [6]. The cold temperatures and their potential influence on hydrates, increased wax deposition, and oil pour point issues may economically and technically limit the ability to perform periodic pressure tests on a development's pipeline systems.

#### **2.2.1.6 Pressure Wave / Acoustic Wave Monitoring**

Pressure wave / acoustic wave leak detection systems monitor the pipeline for the rarefaction wave generated by the onset of a leak. When a leak starts, a drop in pressure occurs nearby at the leak and travels at the speed of sound through the fluid to both ends of the pipeline. Monitoring this pressure change when it reaches the pressure transmitters at each end of a pipeline allows for detection and location of a leak. Pressure trend monitoring systems can also notice this event.

However, pressure wave monitoring systems that solely rely on the pressure wave, as opposed to more indirect changes in the historical pressure trends, may not detect as small of a leak as pressure trend monitoring systems. Once the wave passes, pressure wave / acoustic monitoring systems can no longer detect the leak [6]. Therefore, pressure trend monitoring systems may perform better for detection of small leaks than pressure wave / acoustic monitoring systems.

## **2.2.2 External Leak Detection Systems**

External leak detection systems rely on detecting fluids, gases, temperatures, or other data that may only be present outside of a pipeline during a leak event.

### **2.2.2.1 Vacuum Annulus Monitoring**

Vacuum annulus monitoring includes monitoring the vacuum pressure within the annulus between an inner and outer pipe for a pipe-in-pipe pipeline. To reduce the number of sensors, sensor connections, and cabling along the length of an offshore pipeline, monitoring of a continuous annulus at one end of the pipeline is desired. While this system does not have a limiting leak detection threshold, the application of this technology is limited by distance and the ability to lift and install larger pipe-in-pipe pipelines that may be bundled to other pipelines [6].

### **2.2.2.2 Hydrocarbon Vapour Sensing Systems**

Vapour sensing system technology includes a semi-impermeable tube installed along the length of a buried pipeline route. The tube allows the passage of hydrocarbon vapours into the tube from the surrounding environment while keeping water and other liquids from passing into the tube and flooding it.

At scheduled intervals, either daily or weekly, a vacuum pump is used to draw air and any gases or hydrocarbon vapours that pass into the tube to a vapour sensor for analysis and alarm signal. Based on the timing of passage of the vapours, the location of the leak along the route can be determined [6]. In addition, there are other methods such as smart pigging, acoustic sensing system, overflight radar based remote sensing.

### **2.2.2.3 Fiber Optic Distributed Sensing Systems**

Fiber optic technologies rely on the fiber optic cable, itself, to act as a continuous, distributed sensor along the length of a pipeline. This is different than using discrete, single point instruments spaced along a pipeline. There are three distributed fiber optic technologies that are available for monitoring a pipeline. They rely on the backscatter of different light bands that are available for fiber optic sensing [6]. They are:

- Distributed Temperature Sensing (DTS) – Raman or Brillouin Backscattering (depending on vendor).
- Distributed Acoustic Sensing (DAS) – Rayleigh Backscattering.
- Distributed Strain Sensing (DSS) – Brillouin Backscattering.

Although the fiber is continuous and acts as a continuous sensor, the fiber optic distributed systems are limited by some factors like; spatial resolution, mothing length and water depth limitation [6].

### **2.3 Review of Conventional Leak Detection Systems**

Early research discussed various experimental techniques using field tests for leak detection, such as those reported by Willsky et al. [14] and Brones et al. [15].

In those early stages, researchers used basic approaches to detect pipeline leaks. These methods were mostly based on limit values to observe some significant system variables. However, these basic methods can only detect leaks at a relatively late stage. In addition, similar LDSs are commonly sensitive to much environmental and operational dissimilarity. Hence, they are predisposed to signaling false alarms. Some other basic methods based on both the parameters and state variable techniques were reported in many studies such as those by Isermann and Freyermuth [16], Isermann [17], Billmann and Isermann [18], [19] and Isermann [20]. However, these methods are deemed costly and time-consuming. Wange et al. [21] developed a method to detect and locate leaks in fluid transport pipelines based on statistical autoregressive modeling, using only pressure measurements. Their method was different from the others' methods which do not require flow measurements. However, this statistical approach fails to discover small leaks and has only been tested using a short experimental pipeline. Liou [22] suggested a leak detection method based on transient flow simulations. The study was developed by numerical simulations and physical laboratory experiments. A comparable method was also developed by Loparo et al. [23] using field experiments on real pipeline data, as the data noise in pressure and flow parameters measurements are considered. The occurrence of noise was found to limit the efficiency of the algorithms to detect leaks and stimulated frequent false alarms. It was determined that additional work is required

to improve the means to avoid noise amplification in similar algorithms. In general, leak detection methods used in pipeline monitoring can be categorized into two major types. Approaches belonging to the first type are primarily based on directly measurable quantities such as inflows, outflows, temperatures and pressures. The second type depends on non-measurable quantities such as model parameters, internal state variables and characteristic quantities of the pipeline system. Approaches of this last type are based on modeling and approximation methods. Most of the previous research in leak detection [8, 9, 14, 15, and 16] has involved the first type of method. In fact, much less consideration has been dedicated to develop methods of the second type.

Other analytical and experimental detection methods were also reported. Lee et al. [24] developed a ceramic-based humidity sensor. The authors engaged a local humidity detection method for the purpose of leak detection in power plants. They showed that the sensor conductivity is increased in response to humidity changes. The analytical and experimental results showed that the ceramic humidity sensor fulfilled the requirements for a leak detection system on central steam line for the application of leak-before-break. Ferrante and Brunone [25] solved the governing equations for transient flow in pressurized pipes in the frequency domain by means of the impulse response method. It was showed that the leak opens the system in terms of energy and hence it performs in the same sense of the friction dropping the values of peaks. The analytical expression of the piezometric head spectrum at the downstream and section of a single pipe system during transients is then derived. The evaluation of the results for a pipe with and without a leak was then proposed as an analytical tool for reliability assessment of pipe system.

Hyun et al. [26] studied the possibility of using ground-penetrating radar as one of the non-destructive testing approaches for detecting fluid leaks in buried transportation pipelines. Mounce et al. [27] developed a neural network knowledge-based system for automatically and continuously monitoring the time series for one or more sensors of a supply pipeline system for normal and abnormal behaviours. The system output was used to raise alarms when failures or leaks are detected. The detection system adopts an empirical model based upon pattern recognition techniques applied to time series data. The model allows the prediction of future values based on a log of time series values.

Moreover, there are three main acoustic leak detection systems. These include acoustic listening devices, leak noise correlators and secured hydrophone systems. While each system has its own qualities, it also has limits, as well. Recently, free-swimming leak detection acoustic method was addressed by D. Kurtz [28]. The concept of the free-swimming stems from the realization of the advantage of placing a sensor very near to the leak was expected to provide a highly sensitive leak detection method. One of the major challenges in designing such a sensor was to run for the sensitive detection of the acoustic signal generated by a leak, with minimal interference from noise generated by the movement of the device as it navigates the pipeline. Mergelas and Henrich [29] developed methods that based on passing acoustic sensor along inside the pipe; notice the point above the leak noise signal was greatest. They indicated that approaches of leak noise correlators, although suitable for small pipes, are not consistent with the case of large diameter pipes.

Gao et al. [30] investigated the behaviour of the cross-correlation coefficient for leak signals measured using pressure, velocity, and acceleration sensors. They showed that pressure responses using hydrophones is significant for measurements where small signal-to-noise ratio, but a sharper peak correlation coefficient can be estimated only if accelerometers are used. The authors verified their theoretical work test data from actual buried pipelines. Gao et al. [31] considered the delay between two measured acoustic signals to determine the position of a leak in buried distribution pipelines. The authors compared different time delay estimators for the purpose of leak detection in buried plastic pipes. The results were tested by experimental results. Results of spectral analysis between two sensors were presented. Also, normalized cross-correlation using various correlation approaches for measured signals was also presented. The equivalence between time and frequency domain methods to estimate time delay has been investigated by Brennan et al. [32], the conditions under which both methods was investigated in view of the objective of determining the position of a leak in distribution pipelines. They presented a new interpretation of the process of cross-correlation for time delay estimation. The results reveal that the time delay estimates and their variances calculated using time and frequency domain methods are almost identical. Verde et al. [33] presented a technique for the identification of two leaks in a pressurized single pipeline, where both transient and static behaviour of the fluid in the leak were considered. The method was used to identify the parameters related to the leaks without requirements of value perturbations.

The study presented a method to identify offline the unknown parameters associated with the existence of multiple leaks in a pipeline based on a combination of transient and steady-state conditions. Their model depended on a set of finite dimension nonlinear models assuming flow rate and pressurized measurements at the extremes of the pipeline. It was found that steady-state conditions of the fluid with multiple leaks can be complemented with a dynamic model to reduce the search interval of the leaks identification issue. Hiroki et al. [34] proposed an enhanced leak detection method for the pipeline networks using dissolved tracer material. The leak point was roughly localized by evaluating a time delay from the injection of the tracer-dissolved water until the actual detection of the tracer by using a mass spectrometer. Yang et al. [35] discussed the different methods for leak detection using acoustic signals in buried distribution pipelines based on the correlation techniques. The method of leak detection using time delay estimation was analyzed and a new proposed method using a principle of leak location based on the blind system identification was proposed to avoid the condition of success of the correlation technique as to have prearranged the accurate distance between the two detection points. The proposed method in their study was applied to some known sources and practical pipelines leak location.

#### **2.4 Pipeline Leakage modeling using CFD approach**

Pipeline leakage studies through computational fluid dynamics (CFD) simulation or numerical approach is relatively a new area. Recent research such as that of Ben-Mansur et al. [36] developed a 3D turbulent flow model using a CFD commercial code to detect small leakages in water supply pipelines.

The length of the pipeline used was 200 cm with a leak size of 1 mm. The CFD application was done on ANSYS FLUENT 6.2 platform. In their results, the pressure noise data were treated with Fast Fourier Transform (FFT) and showed data for different leak locations. The pressure gradient outcomes along the pipeline were displayed using steady-state simulations. Results showed that the leak caused a clear increase in the magnitude and frequency of the pressure signal spectrum. However, the temperature implication was not addressed in the model. In fact, this model was developed to address the city water pipelines in onshore conditions that would differ for subsea pipelines. Another numerical study for oil flow in a Tee-conjunction with oil leakage was performed. In the article, a model with two leaks on a Tee-junction was developed by M. de Vasconcellos Araújo et al. [37]. The influence of the leak on the flow dynamic parameters and the behaviour of the fluid were analyzed using velocity vectors and pressure fields. The core branch was 6 m long and 100 mm in diameter while the subordinate branch had the same diameter and was 3 m long. The study assessed the influence of the leak in the flow dynamics parameters. In the results, there was an insignificant variation of the pressure values with the amount of fluid flowing through it. Also, the study only addressed the single-phase flow condition. A similar numerical simulation model was developed by Zhu et al. [38]; the study presented a numerical model to simulate oil leakage from a dented submarine pipeline. In the study, the effects of hydrocarbon density, leak mass flow rate and leak size were observed using the ANSYS (FLUENT) package.

The study showed how to find the time and distance to be able to see oil spill reaching the water surface, but the study did not consider thermal calculations. Cloete et al. [39] developed a 3D numerical model to simulate the plume and free surface behaviour of a ruptured sub-sea gas pipeline by ANSYS (FLUENT). This study was focused on large gas releases due to ruptures and overlooked the chronic leak releases. Siebenaler et al. [40] conducted an experiment to observe a thermal field's behaviour that resulted from potential underwater leaks through orifices of different sizes. This study was intended to evaluate the Fiber Optic Cable (FOC) technologies based DTS. The study simulated leaks in an underwater environment to understand the physical characteristics of leaks using experimental analysis. The results showed temperatures dropped rapidly as oil spread away from the hot pipeline through the water. However, the study presented a lab-scale experimental analysis with limited leak size scenarios. Also, the study tested only two fluid types separately but did not test the thermal gradient sensitivity to multi-phase flow. Reddy et al. [41] developed a CFD model using COMSOL for a small pipeline section. The study tested the effects of a leak on the pressure and velocity of the city gas pipelines for the transient and steady states. Results presented in the study showed the velocity and pressure profiles for single-phase flow but neglected the multi-phase flow effect. Jujuly et al. [42] developed a 3D numerical model of subsea pipeline leakage using a 3-D turbulent flow model; the pipe length was 8 m, the diameter was 0.322 m and the leak was assumed to be at the top middle of the pipe. The CFD simulation results of the study showed that the flow rate of the fluid leaking from the pipe increased with the operating pressure.

The authors asserted that the temperature near the leak orifice increased in the case of incompressible fluids but dropped quickly for compressible fluids. However, no sensitivity analysis was performed to observe the influence of the temperature around the leak hole in their study. Other CFD studies, by Liang et al. [43] focused only on the phonation principle of the pipeline leakage and characteristics of the sound source but neglected the external ocean water effects on fluid leakage behaviour. Also, De Schepper et al. [44] developed a CFD code just to confirm that CFD codes are capable of calculating the different horizontal multi-phase flow regimes in pipelines. The proposed study is a comprehensive CFD study simulating pipeline leak effects from inside the pipeline to the surrounding ocean water in the model.

## Chapter 3: Theory and Governing Equations

### 3.1 Overview

This chapter reviews the theoretical background of the basic equations describing fluid motion in leaked pipelines. It simplifies how the presented models formulate the general equations governing turbulent fluid flow. The Navier- Stokes equations governing the fluid flow have been employed. These equations have been derived based on the fundamental governing equations of fluid dynamics, called the continuity, the momentum and the energy equations, which represent the conservation laws of physics [9].

### 3.2 Review of Theory

A pressure drop along a leaked pipeline is described in the following illustrated chart in Figure 3-1 [45]. Leaks can affect the transmission of fluids in pipes and change the pipeline internal thermodynamic properties such as fluid Temperature (T), Pressure (P), Mass flow rate (Q) and Velocity (V). These fluctuations are simply recognized by LDS devices installed along the flow line to produce different P, T & Q reading histories at specific flow conditions.

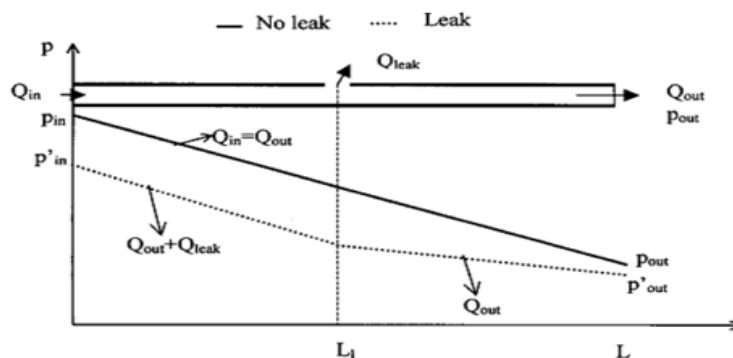


Figure 3-1: Pressure drop along pipeline with and without a leak (after Dinis, 1998)

According to [46], the pressure drop slope decreases linearly from the inlet to the outlet end in a circular pipe and this is denoted as:

$$P_{inlet} - P_{outlet} = \Delta P = C_{pro} L \quad (3.1)$$

where  $L$  is the pipe total length and  $C_{pro}$  is the proportionality constant, which is assumed as:

$$C_{pro} = \frac{8\rho f Q_{out}^2}{\pi^2 D^5} \quad (3.2)$$

where  $\rho$  is the fluid density,  $D$  is the inside pipe diameter,  $f$  is Moody friction factor and  $Q_{out}$  is outlet flow rate:

$$Q_{in} = Q_{out} + Q_{Leak} \quad (3.3)$$

The value of conservation of mass in Equation (3.3) helps in predicting leaks along the flow lines. The outflow mass during a time interval is equal to the mass inflow over the same period under steady-state conditions, and a leak is detected when the variance between the measured inflow and outflow is more than the likely loss in mass, due to flow uncertainty. The pressure change is typically accompanied by a transitory change in velocity. Also, the pressure and velocity variation incline to change with leak size and pipeline processes [45], [46]. According to [47], the formula for a single-phase gas leak in terms of inlet and outlet pressure can be denoted as:

$$q = C_{sp} F_L (p_{in}^2 - p_{Out}^2)^n \quad (3.4)$$

where  $q$  is the outlet gas flow rate (m<sup>3</sup>/s),  $C_{sp}$  is a constant for a specific pipe,  $m$  is normally 0.5 and  $F$  is the efficiency drop due to a leakage, which can be used in detecting the leak's existence. Hence,  $F$  is given as:

$$F = \{1 + L_h(q_h^2 + 2q_h)\}^{-n} \quad (3.5)$$

The unit-less leak location and leak rate are given as:

$$L_h = \frac{D_h}{L_p} \quad (3.6)$$

$$q_h = \frac{q_L}{q} \quad (3.7)$$

where  $L_p$  the pipeline length,  $D_h$  is the distance to the leak hole and  $q_L$  is the leak rate [47].

For multi-phase flow in a pipe with a leak, Scott et al [47] asserted that the outlet gas flow rate can be denoted as a function of inlet and outlet pressure in the following formula:

$$q_m = F_{Leak}(F_{2-\phi})_q \left( \frac{CZTf_{sg}L_p}{d^5} \right)^{-0.5} (p_{in}^2 - p_{out}^2)^{0.5} \quad (3.8)$$

where  $q_m$  is the outlet gas flow rate at the multi-phase flow condition (m<sup>3</sup>/s),  $C$  is constant,  $Z$  is the real gas compressibility factor,  $T$  is temperature,  $d$  is the diameter of the pipe and  $f$  is friction factor. The symbol  $sg$  denotes single-phase conditions.

The additional term ( $F_{2-\phi}$ ), which is called the two-phase efficiency, is assumed as:

$$F_{2-\phi} = \frac{(dp/dx)_{sg}}{(dp/dx)_{2-\phi}} \quad (3.9)$$

The additional two-phase flow dependent term ( $F_{2-\phi}$ ) in Equation (3.9) above differentiates the single-phase flow from the multi-phase flow for a leaking pipe and this makes it harder to detect a leak in a multi-phase flow [46], [47].

To describe the thermal profiles of hydrocarbon mixtures in the subsea pipelines, mass, momentum and energy conservation equations for each phase are presented below. The Darcy-Weisbach equation is usually applicable for liquids and incompressible flow. The hydrodynamic model offers the Darcy-Weisbach loss model approach as the default method for describing pipe frictional losses [48], expressed in Equation (3.10):

$$\Delta P = f \frac{L}{D} \rho \frac{u^2}{2g} \quad (3.10)$$

where  $f$  is the Moody friction factor, a function of the Reynolds number ( $Re$ ) and pipe roughness. It is defined as the ratio of inertial to viscous forces. Flow in a circular cylinder varies with the Reynolds number. Small Reynolds number corresponds to slow viscous flow where frictional forces are dominant. Fluid flow regimes are in-between laminar and turbulent. When Reynolds number increases, the flow regime is categorized by the Reynolds number which is a fundamental characteristic dimensionless parameter for a fluid [49]. Flows are characterized by rapid regions of velocity variation and the occurrence of vortices and turbulence [50].

For laminar flow, the hydrodynamic model uses the standard laminar Equation (3.11) to calculate the Moody friction factor as:

$$f = 64/Re \quad (Re < 2100) \quad (3.11)$$

The Reynolds number ( $Re$ ) can be expressed in Equation (3.12):

$$Re = \rho v D / \mu \quad (3.12)$$

For low  $Re$  ( $<2100$ ), the viscous force causes the flow to remain in the laminar regime. In the case of high  $Re$  ( $>4000$ ), the non-linear interactions force the flow to a chaotic condition that is the turbulent regime. Between these limits is the transient condition. The Colebrook-White iterative friction factor equation is used to obtain friction factors in the turbulent flow regime [48], presented in Equation (3.12):

$$f = \left( 1.14 - 2 \log \left( \frac{e}{D} + \frac{9.35}{Re \sqrt{f}} \right) \right)^{-2} \quad (Re > 4000) \quad (3.13)$$

Flow becomes very irregular with instabilities beyond Reynolds number of 200,000.

### 3.3 Hydrodynamic model governing equations

The focus of this study is turbulent flow, as it is believed that the flow condition in the field's pipelines is mostly in the transient or turbulent condition.

The main equations describing the turbulent fluid flow in pipes result from an equation of momentum, an equation of continuity, equation of energy and equation of state [48], [51], [52]. In general, the governing equations are expressed as given in Equations (3.14-3.19):

Continuity equation:

$$\frac{\partial \rho}{\partial t} + \frac{\partial(\rho V)}{\partial x} = 0 \quad (3.14)$$

where  $V$  is the flow velocity, and  $\rho$  is the density of gas. Substituting  $M = \rho v A$ , produces:

$$\frac{\partial \rho}{\partial t} + \frac{1}{A} \frac{\partial M}{\partial x} = 0$$

where  $M$  is the mass flow,  $A$  is the cross-sectional area of the pipe.

Momentum equation:

$$-\frac{\partial P}{\partial x} - \frac{2 F \rho v^2}{D} - (g \rho \sin(\alpha)) = \frac{\partial(\rho v)}{\partial t} + \frac{\partial(\rho v^2)}{\partial x} \quad (3.15)$$

where  $g$  is the acceleration of gravity,  $\alpha$  is the angle between the horizon and the direction  $x$ . The  $F$  is Fanning friction coefficient, calculated for every discrete section of the pipeline, as illustrated by Nikuradse and Reichert in Equations (3.16) and (3.17) below [53]. The constituent factors  $(\partial/\partial t (\rho u))$ ,  $((2f\rho u^2)/D)$ ,  $(g \rho \sin (\alpha))$  and  $(\partial/\partial x(\rho u^2))$  define the gas inactivity, the force of hydraulic friction, the gravity force and the flowing gas dynamic pressure, respectively.

$$F = 16/Re \quad (Re < 2100) \quad (3.16)$$

$$\frac{1}{\sqrt{f}} = -3.6 \log \left( \left( \frac{6.9}{\text{Re}} + \frac{\epsilon/D}{3.7} \right) \right)^{10/9} \quad (\text{Re} > 4000) \quad (3.17)$$

where  $\epsilon$  is the roughness of the inner pipe surface,  $D$  is the inner pipe diameter. The  $\epsilon/D < 0.05$  factor must be considered for  $f$  calculation by Equation (3.17).

Energy equation:

$$\begin{aligned} \frac{\partial}{\partial t} [(\rho A dx)(c_v T + \frac{1}{2}v^2 + gz)] \\ + \frac{\partial}{\partial x} \left[ (\rho v A dx)(c_v T + \frac{P}{\rho} + \frac{1}{2}v^2 + gz) \right] = q \rho A dx \end{aligned} \quad (3.18)$$

where  $T$  is the gas temperature,  $q$  is the heat addition per unit mass per unit time, and  $c_v$  is the specific heat at constant volume.

Equation of state:

$$P = Z \rho R T \quad (3.19)$$

The field conditions are commonly transient or turbulent. Hence, the steady-state hydrodynamic model is not represented in this study. However, the steady state is still considered as the basic scenario for the model's first checkup.

### 3.3.1 Steady-state in the hydrodynamic model

The temperature of the gas is calculated using the heat balance equation. According to [52], the heat transfer process is assumed to be in a quasi-steady-state.

The heat equation can be expressed as in Equation (3.20):

$$C_p M dT = -k_L(T_{gas} - T_{amb})dx \quad (3.20)$$

where  $C_p$  is the specific heat at persistent pressure, J/kg K;  $M$  the mass flow, kg/s;  $k_L$  the heat transfer coefficient, W/m K;  $T_{gas}$  the gas temperature, K; and  $T_{amb}$  is the ambient temperature, K.

The Energy equation (3.18) that describes the fluid flow in the horizontal pipe can be rearranged for the steady-state condition as in Equation (3.21), where the first part of  $\frac{\partial}{\partial t}[(\rho A dx)(c_v T + \frac{1}{2}U^2 + gz)] = 0$  and is restated as below:

$$\frac{\partial}{\partial x} \left[ (\rho V A dx) \left( c_v T + \frac{P}{\rho} + \frac{1}{2}V^2 + gz \right) \right] = q \rho A dx \quad (3.21)$$

Eventually, the energy equation in the formula of the heat balance equation can be calculated by Equation (3.20), written in the form below:

$$\frac{dT}{T_{gas} - T_{amb}} = \frac{-k_L}{C_p M} dx$$

Resolving the equation by integrating  $T(0)$ , ( $T_{x=0}$ ) and  $T(x)$ ,  $x \in (0, L)$  produces:

$$\int_{T(0)}^{T(x)} \frac{dT}{T_{gas} - T_{amb}} = \frac{-k_L}{C_p M} \int_0^x dx$$

This is resolved to:

$$T(x) = T_{amb} + (T(0) - T_{amb})e^{-\beta x} \quad (3.22)$$

where  $\beta = k_L / (c_p M)$

The pressure at a certain point of the pipe can be expressed by the following equation:

$$p(x) = \sqrt{(p(0))^2 - K \times M^2} \quad (3.23)$$

where  $M$  is the mass flow,  $kg/s$ ;  $p(0)$  is the pressure at  $x=0$ ,  $Pa$ , and  $K$  is the coefficient, defined by the following equation:

$$K = \frac{ZR}{A^2} \left[ \frac{4F}{D} \left( T_{amb}x + \frac{T(0) - T_{amb}}{\beta} + \frac{T(0) - T_{amb}}{\beta} e^{-\beta x} \right) - 2(T(0) - T(x)) \right] \quad (3.24)$$

where  $x$  is the spatial coordinate,  $m$ ;  $Z$  the compressibility factor;  $F$  is the Fanning friction coefficient;  $R$  the specific gas constant,  $J/kg K$ , and  $A$  is the cross-sectional area of the pipe,  $m^2$ .

### 3.3.2 Transient flow in the hydrodynamic model

The temperature profile is calculated as a function of pipeline distance. In this case, the transient and thermal flow of gas in a horizontal pipe ( $\rho g \sin \alpha = 0$ ),  $((\partial/\partial x (\rho v A g z dx)) = 0)$  is defined by the system of Equations (3.14)– (3.19) above. The intended models are obtained by overlooking some terms in the basic equation to keep it simple. This results from the quantitative approximation of elements of the equation, under some given conditions of the process of the pipeline. An essential condition for appropriate selection of the model is consequently the earlier breakdown of these conditions.

In this model, the energy equation is simplified by assuming that the heat transfer is partial to conduction through a walled tube and the fluid along a pipeline, the equation can be expressed as:

$$q\rho A dx = A \frac{\partial}{\partial x} \left( \Phi \frac{\partial T}{\partial x} \right) dx - k_L (T_{gas} - T_{amb}) dx \quad (3.25)$$

where  $\Phi$  is the thermal conductivity coefficient of fluid,  $W/m K$ , and  $k_L$  is the heat transfer coefficient,  $W/m K$ .

By combining the two Equations (3.18) and (3.25), the concluding version of the equation can be expressed as the following formula:

$$\begin{aligned} \frac{\partial}{\partial x} (\rho V A c_v T dx) + \frac{\partial}{\partial x} \left( \frac{\rho V A P}{\rho} dx \right) + \frac{\partial}{\partial x} \left( \frac{\rho A V^3}{2} dx \right) \\ + \frac{\partial}{\partial x} (\rho V A g z dx) - \frac{\partial}{\partial x} \left( \Phi A \frac{\partial T}{\partial x} dx \right) \\ + k_L (T_{gas} - T_{amb}) dx + \frac{\partial}{\partial t} (\rho V A c_v T dx) \\ + \frac{\partial}{\partial t} \left( \frac{\rho A V^2}{2} dx \right) + \frac{\partial}{\partial t} (\rho A g z dx) = 0 \end{aligned} \quad (3.26)$$

This can only be a starting point with the assumption that, in the case when the designated parameters do not change quickly, transient thermal flow in the horizontal pipe can be summarized in the set of governing Equations (3.27.1- 3.27.4) as in Table 3-1[52].

**Table 3-1: Condensate compositions mole fraction**

$$\frac{\partial \rho}{\partial t} + \frac{\partial(\rho V)}{\partial x} = 0 \quad (3.27.1)$$

$$\frac{\partial P}{\partial x} + \frac{\partial(\rho V)}{\partial t} + \frac{\partial(\rho V^2)}{\partial x} + \frac{2f\rho V^2}{D} = 0 \quad (3.27.2)$$

$$\frac{\partial}{\partial x}(\rho V A c_v T dx) + \frac{\partial}{\partial x}\left(\frac{\rho V A P}{\rho} dx\right) + \frac{\partial}{\partial x}\left(\frac{\rho A V^3}{2} dx\right) + \frac{\partial}{\partial x}(\rho V A g z dx) - \frac{\partial}{\partial x}\left(\Phi A \frac{\partial T}{\partial x} dx\right) + k_L(T_{gas} - T_{amb}) dx + \frac{\partial}{\partial t}(\rho V A c_v T dx) + \frac{\partial}{\partial t}\left(\frac{\rho A V^2}{2} dx\right) + \frac{\partial}{\partial t}(\rho A g z dx) = 0 \quad (3.27.3)$$

$$\frac{P}{\rho} = Z\rho RT \quad (3.27.4)$$

In this work, the flow regime for the CFD calculations is considered at the transient condition in a horizontal pipe with a leak at the top. Fluids are assumed constant in density. The walls are No-slip and have constant friction factor that is calculated using the Churchill Equation (3.28), [44], [54] presented below:

$$f = 8 \left( \left( \frac{8}{Re} \right)^{12} + (A + B)^{-1.5} \right)^{1/12} \quad (3.28)$$

where A and B as:

$$A = \left( -2.457 \ln \left( \left( \frac{7}{Re} \right)^{0.9} + 0.27 \left( \frac{e}{D} \right) \right) \right)^{16}$$

$$B = \left( \left( \frac{37530}{Re} \right) \right)^{16}$$

### **3.4 CFD Model governing equations**

#### **3.4.1 Pre-analysis**

A turbulent flow shows small-scale fluctuations in time. It is usually not possible to resolve these fluctuations in a CFD calculation. So the flow variables such as velocity, pressure, etc. are time-averaged. The k- $\epsilon$  model consists of two differential equations: one each for the turbulent kinetic energy k and turbulent dissipation  $\epsilon$ . These two equations have to be solved along with the time-averaged continuity, momentum and energy equations.

#### **3.4.2 CFD k- $\epsilon$ turbulence model**

The governing equations for the pipe flow for the CFD model are expressed by the Navier-Stokes equation. Claude Navier and George Stokes developed the well-known equations of fluid motion, known as the Navier-Stokes equations. These governing equations have been derived from the basic governing equations of fluid dynamics, named the continuity, the momentum and the energy equations, that represent the conservation laws of physics [9], [11], [41], [55]. The k- $\epsilon$  turbulence model resolves the flow based on the statement that the rate of production and dissipation of the turbulent state are in near-balance in an energy transfer. The basic two-transport-equation model solves for kinetic energy (k) and turbulent dissipation ( $\epsilon$ ). Turbulent dissipation is the rate at which velocity fluctuations dissipate. Coefficients are empirically derived and valid for fully turbulent flows only.

In the standard k-ε model, the eddy viscosity is obtained from a single turbulence length scale, so the intended turbulent diffusion occurs only at certain scales, whereas all scales of motion will join the turbulent diffusion. The k-ε model uses the gradient diffusion hypothesis to link the Reynolds stresses to the mean velocity gradients and the turbulent viscosity [56], [57]. K-ε is used to describe the field quantities of velocity scale  $\vartheta$  and length scale  $\ell$ , illustrative of the large-scale turbulence, as follows:

$$\vartheta = K^{1/2} \quad \ell = \frac{k^{3/2}}{\varepsilon}$$

where  $k$  is turbulent kinetic energy and  $\varepsilon$  is the turbulent kinetic energy dissipation. The field quantities  $k$  and  $\varepsilon$  are random functions of space and time; their average representation can provide adequate information about the fluid flow [10], [58].

$$\mu_t = C\rho\vartheta\ell = \rho C_\mu \frac{k^2}{\varepsilon} \quad (3.39)$$

The governing transport equations for  $k$  and  $\varepsilon$  of the standard k - ε model is presented by Reynolds-averaged Navier-Stokes (RANS) as below.

The kinetic energy of turbulence model can be described as:

$$\frac{\partial(\rho k)}{\partial t} + \frac{\partial(\rho k v_i)}{\partial x_i} = \frac{\partial}{\partial x_j} \left( \frac{\mu_{eff}}{\sigma_k} \frac{\partial k}{\partial x_j} \right) + G_k - \rho\varepsilon \quad (3.40)$$

The dissipation rate of kinetic turbulent energy can be modeled as:

$$\frac{\partial(\rho\varepsilon)}{\partial t} + \frac{\partial(\rho\varepsilon v_i)}{\partial x_i} = \frac{\partial}{\partial x_j} \left( \frac{\mu_{eff}}{\sigma_\varepsilon} \frac{\partial \varepsilon}{\partial x_j} \right) + C_{\varepsilon 1} \frac{\varepsilon}{k} (G_k + C_{\varepsilon 2} G_b) - C_{\varepsilon 2} \rho \frac{\varepsilon^2}{k} \quad (3.41)$$

where  $G_k$  and  $G_b$  characterize the generation of turbulence kinetic energy due to the mean velocity gradient and due to buoyancy respectively. The buoyancy effects on  $\varepsilon$  are often neglected in the transport equation for  $\varepsilon$ . Then,  $G_k$  can be substituted as:

$$G_k = -\rho \overline{v_i v_j} \frac{\partial v_j}{\partial x_i}$$

Equations (3.39) to (3.41) include five adjustable constants, based on an extensive check of a wide range of turbulent flows; the parameters included in the equations have the following values:

$$C_{\varepsilon 1} = 1.44, \quad C_{\varepsilon 2} = 1.92, \quad C_\mu = 0.09, \quad \rho_k = 1.00, \quad \rho_\varepsilon = 1.30$$

### 3.4.3 Computational details

In the current work, RANS models such as the k- $\varepsilon$  model have been chosen to test the suitability and the applicability of the model on the flow in pipes for Reynolds number of 10000. The RANS models used here employ a finite volume method (FVM) to discretize computational domain utilizing fine meshing. A structured quadrilateral mesh is employed in these simulations. The mesh creates finite volumes which are used to solve the mass, and momentum, equations. Discretization helps to linearize a large system of non-linear algebraic conservation and transport equations.

The structured mesh is generated using STAR-CCM 12. Near to the cylinder wall, the very fine mesh is required to resolve boundary layer separation. Quadrilateral cells would form the grid structures around the cylinder.

### **3.5 Summary**

The overall simulation work was split into two simulation studies. The first simulation is detailed in chapter 4, describes a hydrodynamic model that to study the pipeline fluid flow system performance. The hydrodynamic model can help to find the most critical conditions along the entire pipeline system. This model is developed to overcome the challenges of simulating pipeline leakage underwater for long-distance pipelines. In the second simulation, the most critical segment among the whole system is studied using CFD model. The CFD model is presented in chapter 5, to understand the fluid flow behaviour in leaking pipelines as well as their effects on the surroundings.

## **Chapter 4: Offshore Pipelines Hydrodynamic Simulation**

### **4.1 Overview**

The hydrodynamic model helps to find the most critical conditions along the entire pipeline. This model is developed to overcome the challenges of simulating pipeline leakage underwater for long-distance pipelines. Required data and initial conditions are collected to develop a desired initial boundary condition case and a fluid properties package for the model. Then, the proposed hydrodynamic model is developed. The pressure and temperature profiles assessment are conducted to select the segment in the most critical condition in the pipeline. This model examines a long-distance of a subsea pipeline to assess the fluid flow properties (e.g. temperature, pressure, etc.), the most extreme behaviour in the pressure and temperature profiles are then selected. Low computation applications which estimate the dynamics of single-phase and multi-phase fluids are able to capture the temperature dynamics for steady and transient conditions.

### **4.2 Methodology of the Hydrodynamic Simulation**

The hydrodynamic simulation is presented as the first stage in the overall methodology in Figure 4-1. A hydrodynamic model is created using Applied Flow Technology (AFT) software as in the following steps:

1. Collect the initially available information and the boundary conditions of the system.
2. Create fluid properties package (i.e. temperature, pressure, density and viscosity) based on the case information (i.e. fluid type, fluid flow regime and phase flow condition).

3. Set up the pipeline system that includes pipe sizes, lengths and elevations for the developed case.
4. Create and run the hydrodynamic model to observe and identify the most extreme behaviour in the model parameters (e.g. pressure, temperature and fluid flow velocity)
5. Evaluate the pressure and temperature profile results along the entire length of the pipeline based on the inlet specifications. From these hydrodynamic model results, the most critical segment of the pipeline is selected.
6. Define the boundary conditions of the selected critical segment to be used in the detailed CFD study.

Typically, the segment where temperature and pressure are the lowest is selected for the CFD study. Required data and boundary conditions are obtained from the hydrodynamic model for a further CFD simulation study in the second stage.

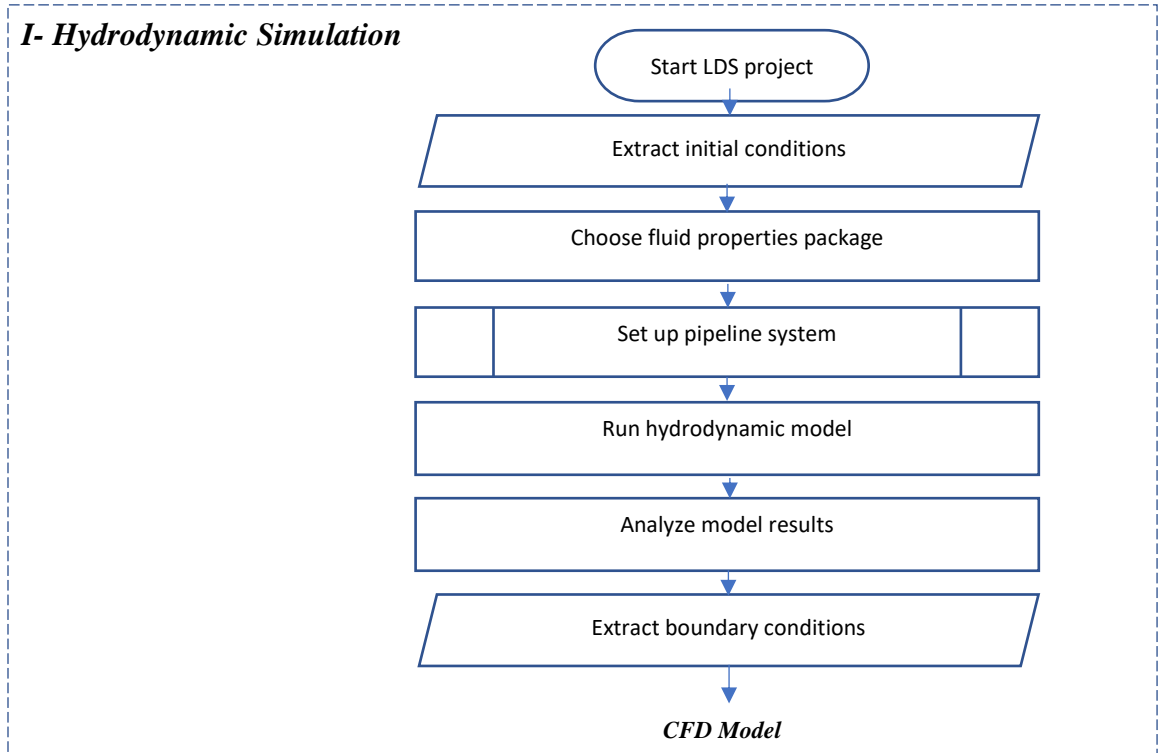


**Figure 4-1: Procedures of hydrodynamic simulation by steps to study the pipeline leak and its impact on sea water**

### 4.3 Applications of the Methodology

To demonstrate the proposed methodology, an offshore pipeline with the following dimensions and conditions is considered: the length of the pipeline is 150 km, ID 25 cm; the thickness is 0.4508 cm with 4 pipe segments of the lengths of 30 km, 100 km, 10 km and 10 km, and there are 3 joints (J3, J4 and J6) elevated at heights 0 m, 0 m and 10 m from the left to the right side, respectively, as shown in Figure 4-2.

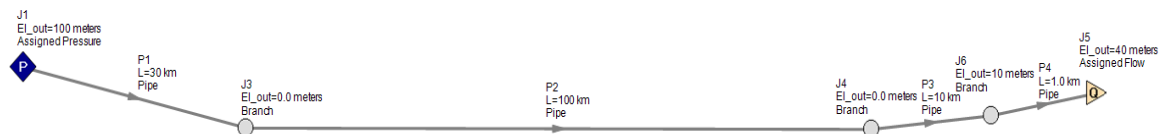


**Figure 4-2: Hydrodynamic physical model components**

The pipeline has various elevation levels, to emulate real subsea basin raises. The pipeline is fixed with a pressure-driven inlet node (J1) at 100 m elevation and a mass flow rate driven outlet node (J5) at 20 m on the other end. The fluid systems are developed in single-phase flow for water and multi-phase flow for gas condensate. Additionally, the fluid properties are obtained from the literature according to the work considered in the input data reported by INTECSEA group experiments for testing the Fiber Optic Cable Distributed Sensing of LDSs in arctic and cold regions by Thodi et al. [4] and Afebu et al.[46]. The hydrodynamic model is created using AFT software; the required fluid properties package is set in the application system. Then, the model input data are collected according to the proposed model requirements as detailed in Table 4-1.

**Table 4-1: Input fluid properties and initial boundary condition for hydrodynamic model**

<b>Fluid properties</b>	<b>Single-phase Flow</b>	<b>Multi-phase Flow</b>
Fluid Type	Water	Condensate
Pipe Material	ANSI Steel	ANSI Steel
Absolute Roughness	0.004572 cm	0.004572 cm
Pipe Diameter	25 cm	25 cm
Pipe Thickness	0.4508 cm	0.4508 cm
Pipe Total Length	150 km	150 km
Pipes Elevations	0 -100 m	0 - 100 m
Initial Inlet Pressure	586 Bar	586 Bar
Initial Inlet Temperature	20.0 °C	20.0 °C
Ambient Temperature	4.0 °C	4.0 °C
Initial Flow Rate	192.8 kg/sec	495.2 kg/sec
Density	998.3167 kg/m <sup>3</sup>	352.4468 kg/m <sup>3</sup>
Viscosity	0.00177 Kg/ sec-m	3.562E-05 Kg/ sec-m

After the input data is entered, the model is run to calculate the results. Based on the pressure and temperature profiles results, a segment of the pipeline is selected where the pipeline pressure and temperature are close to the minimum, remote from both ends of the pipeline, thus posing the most challenging situation.

Details of the selection criteria are presented in the study discussion below. According to Tafreshi et al. [59], temperature dynamics are significantly different for single-phase and multi-phase fluid flow cases. Therefore, the proposed hydrodynamic model considers the implication of the phase flow variation. A selective PVT file covering the fluid's compositional properties is defined in Table 4-2. The file is created using PVTSIM software and has been used on the hydrodynamic model and then in the CFD calculations, reported from [34], [46], [60], [61].

**Table 4-2: Condensate compositions (mole fraction), after Saleh and Stewart [59]**

Component	Gas mol %	Liquid mol %
N2	0.15	0
CO2	0.18	0
H2S	0	0
CI	87.98	0
C2	5.29	0.1
C3	2.83	0.07
i-C4	0.68	0.06
n-C4	0.91	0.13
i-C5	0.41	0.21
n-C5	0.31	0.25
C6	0.56	1.73
C7+	0.7	97.45
TOTAL	100	100
Liquid density (IB/FT3)	50.067	
Liquid MW		156.37
Gas gravity (air = 1)	0.802	

As described in the methodology (refer to Figure 4-1), the final step in the hydrodynamic simulation is to transfer the output results of the selected segment boundary condition to the CFD model including fluid properties for both single-phase and multi-phase cases. The results disclose the responses to extreme temperature, pressure and velocity profiles along the pipeline, shown in the results discussion below in Figures 4-3, 4-4 and 4-5. The outputs from the hydrodynamic model are used for a sophisticated CFD simulation in the next chapter.

## 4.4 Simulation Results

### 4.4.1 Boundary Condition Assessment by Hydrodynamic Model

The proposed hydrodynamic model for the 150 km pipeline length provides the temperature, pressure and velocity profiles for the entire pipeline in a turbulent flow condition. From these profiles, the most critical (e.g. peaks, drops) parts of the pipeline are selected according to the distance from the inlet for the limiting conditions. The results from the hydrodynamic model for the single phase and multi-phase cases are shown in Figures 4-3, 4-4 and 4-5 respectively. According to these figures, the most critical segments are deemed to be at 30 km from the inlet in both cases. The temperature profiles show a critical temperature drop at 30 km; the multi-phase flow shows a greater drop than the single-phase case. Also, as shown in the velocity charts, the velocity sags at 30 km. Similarly, the multi-phase velocity has a much more significant drop than the single-phase does. However, the critical segment distance is the same for both cases, at the same other parameters.

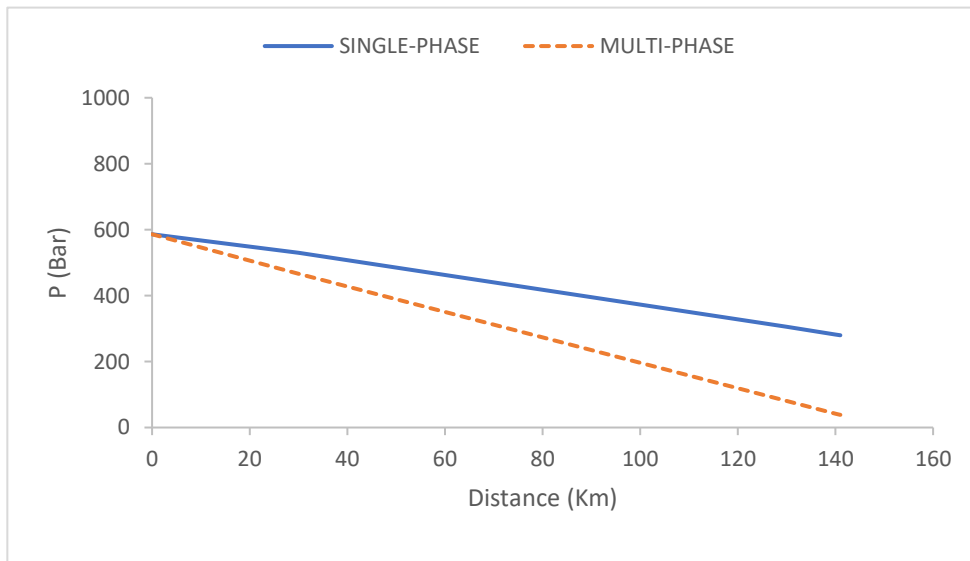
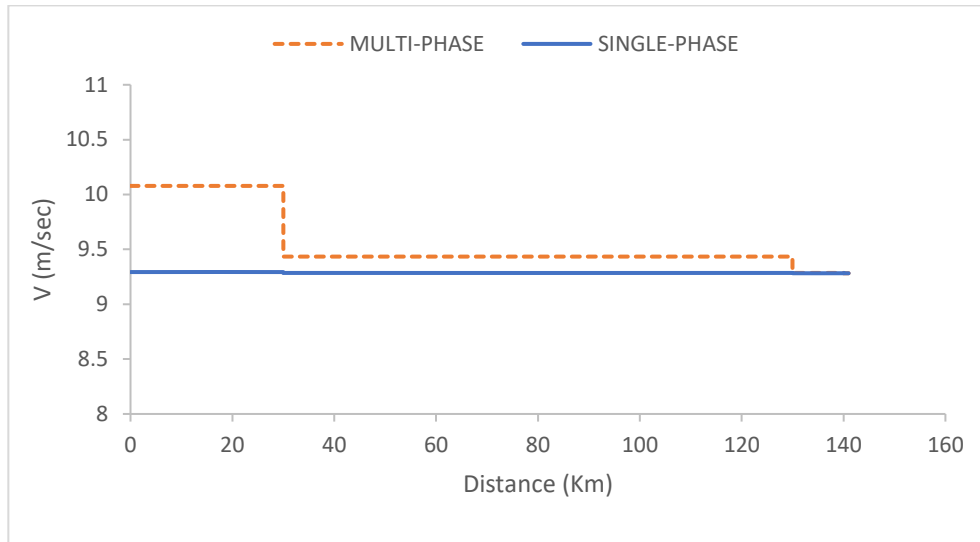
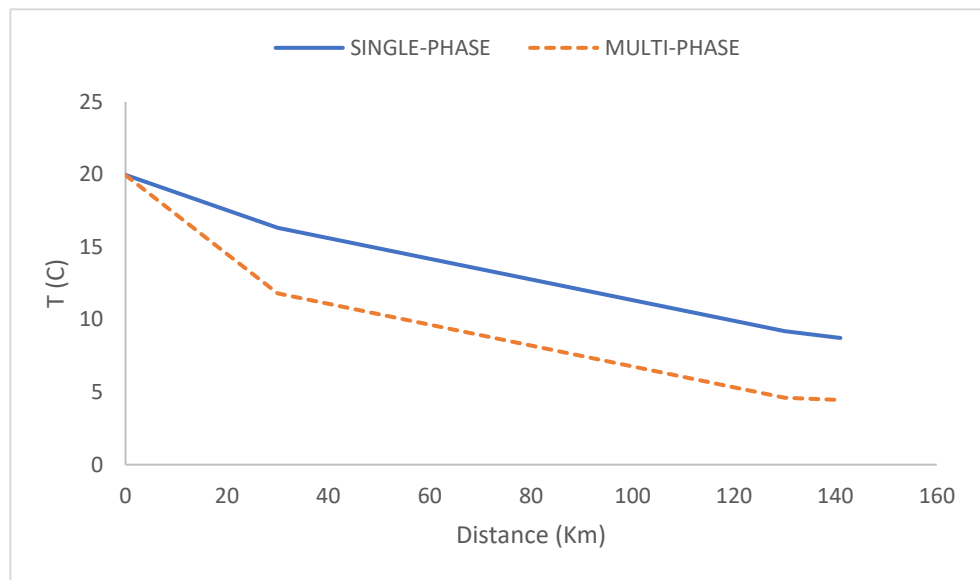


Figure 4-3: Pipeline pressure profiles of the hydrodynamic model in single-phase and multi-phase flow



**Figure 4-4: Fluid flow velocity profiles of the hydrodynamic model for single-phase and multi-phase flows**



**Figure 4-5: Pipeline fluid temperature profiles of the hydrodynamic model for single-phase and multi-phase flows**

The fluid properties and critical segment information for single-phase flow and multi-phase flow are shown below in Table 4-3. The field data and boundary conditions required for the CFD simulation are determined from the hydrodynamic model's outcomes. This information is considered as an initial condition for the CFD model.

**Table 4-3: Fluid properties and critical segment information**

<b>Properties</b>	<b>Single-phase Flow</b>	<b>Multi-phase Flow</b>
Fluid Type	H2O	Gas Condensate
Pipe Inner Diameter	0.25 m	0.25 m
Critical Segment Position	30 km	30 km
Critical Segment Temperature	16 °C	12 °C
Critical Segment Velocity	9.15 m/sec	9.53 m/sec
Inlet Temperature	20 °C	20 °C
Ambient Temperature	4.0 °C	4.0 °C
Inlet Pressure	586 bar	586 bar
Total Inflow	192.8 kg/sec	495.2 kg/sec
Total Outflow	192.8 kg/sec	495.2 kg/sec
Density	998.3167kg/m3	352.4468 kg/m3
Viscosity	0.0017 kg/sec-m	3.562E-05 kg/sec-m
Total Energy Inflow	39,751 kW	187,214 kW
Total Energy Outflow	17,460 kW	160,397 kW

The most critical segment is suggested for a sophisticated CFD simulation based on the most extreme condition of the 150 km of the pipeline. The hydrodynamic model provides the initial required parameters and boundary conditions for the following CFD simulation in the next chapter.

## **Chapter 5: Pipeline Leakage Computational Fluid Dynamics Simulation**

### **5.1 Overview**

CFD modeling formulates mathematical physics problem formulation in the form of Partial Differential Equations (PDEs) with appropriate boundary conditions and initial conditions. Modeling may include: geometry and domain, coordinates, governing equations, flow conditions, initial and boundary conditions. CFD computations are usually very expensive, requiring parallel high-performance supercomputers with their use of multi-block technique [10]. In this study, the CFD model is used to simulate the response of temperature and pressure sensitivity along the subsea pipeline to leaks of different sizes. The turbulent simulations have been carried out using a  $k-\varepsilon$  turbulence model and the multi-phase interaction has been tested. Also, the coupled energy model is used in the model's solver which is an extension of the coupled flow model. Together, they solve the conservation equations for mass, momentum, and energy simultaneously

### **5.2 Methodology of the CFD Simulation**

The results from the full-length hydrodynamic simulation model have been used for the second simulation such as the initial condition parameters needed to create a section of leaked pipeline model using CFD applications. The unique role of this work is to develop a comprehensive model that would simulate the fluid flow through a leaked pipeline into the flowing ocean water in one model. Therefore, a methodology of CFD simulation is developed as shown in Figure 5-1. The procedures of the methodology aim to determine the effect of leak size on temperature and pressure changes around the leak soundings,

as well as the effect of fluid flow types and compositions. The following CFD study steps are carried out:

1. Obtain the fluid flow properties and the model boundary conditions from the past hydrodynamic model results.
2. Create and run the model by using CFD (STAR-CCM 12.4) software package.
3. Test and validate the model with previous works to check the credibility of the model.
4. Calculate the solution based on the fluid flow case (i.e. single-phase or multi-phase flow) and the flow regimes (i.e. steady-state or transient conditions).
5. Generate the pressure and temperature profiles for different leak sizes in the CFD model to study the effect of leak size changes in both single-phase and multi-phase conditions.
6. Display the temperature changes ( $\Delta T_{leak}$ ) obtained from the temperature profile for different leak sizes to carry out the temperature sensitivity analysis.

This simulation' results can help to characterize the specifications needed to design DTS technologies projects.

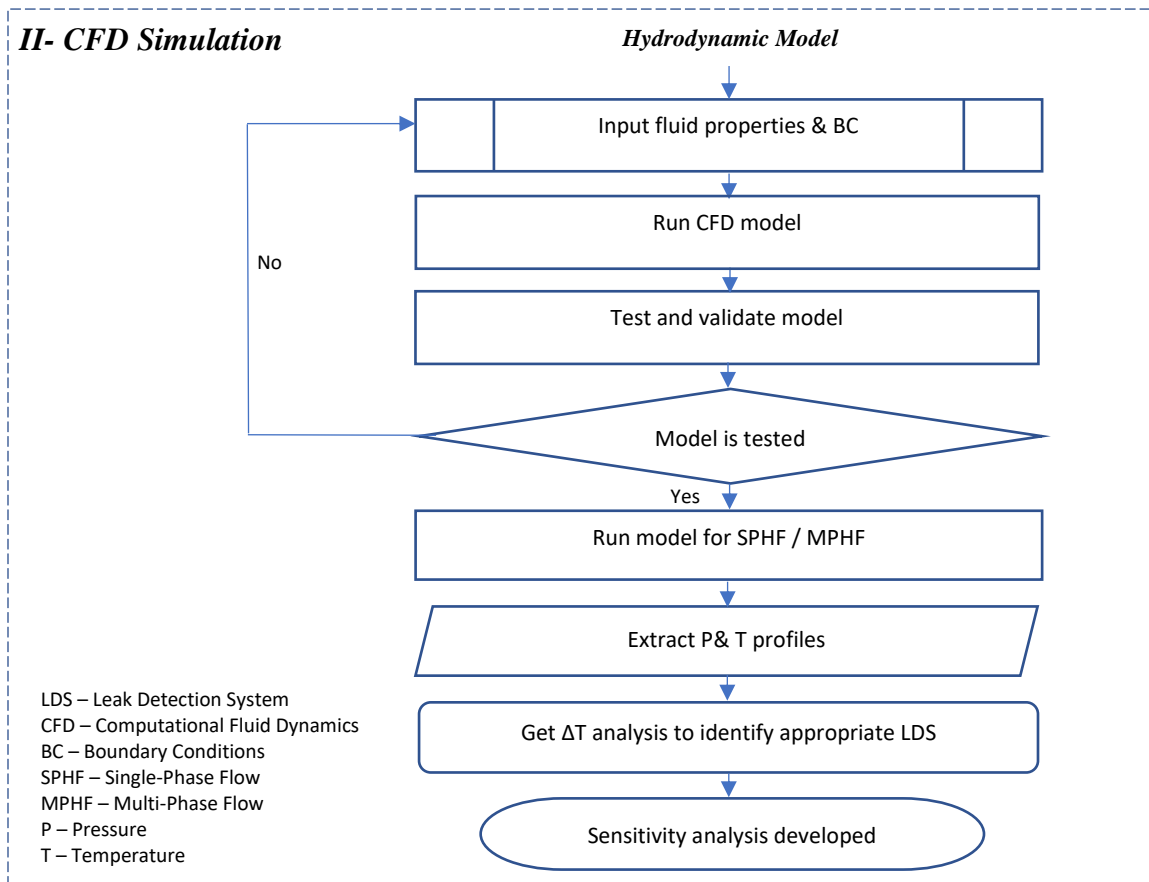


**Figure 5-1: Procedures by steps to study the pipeline leak and its impact on sea water**

### 5.3 Application of the Methodology

The model of the pipeline and the surrounding water domain was illustrated in the sketch showing the leak hole as in Figure 5-2. The pipe length is assumed  $L = 1.0$  m, the inner diameter  $ID = 25$  cm. The leak is assumed to be located at the top of the pipe ( $x = L/2$ ,  $y = D/2$ ,  $z = 0$ ). Leak hole sizes considered for the study are 2, 4, 6, 8, 10, 12 and 14 mm. The pipe was submerged under moving ocean water and assumed 0.1 m/s.

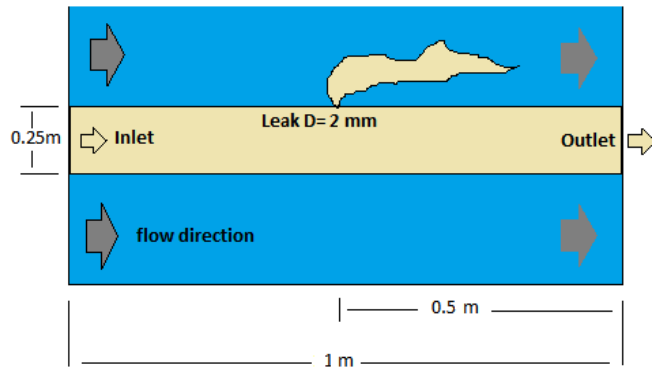


**Figure 5-2: Pipeline physical model and leak position**

The model geometry of the pipeline and the surrounding water domain was created using SolidWorks package and imported to the STAR-CCM software. An isometric view of the pipeline geometry with a zoomed view of the leak hole is shown in Figure 5-3. The flow domain of the pipe length assumed  $L = 1.0$  m, the inner diameter  $ID = 25$  cm and the pipe is 0.45 cm thick. The leak is assumed to be of a circular shape and located at the top of the pipe ( $x = L/2$ ,  $y = D/2$ ,  $z = 0$ ). Leak sizes considered for the study are 2, 4, 6, 8, 10, 12 and 14 mm. The pipe was assumed submerged underwater in a tank of 100x85 cm.

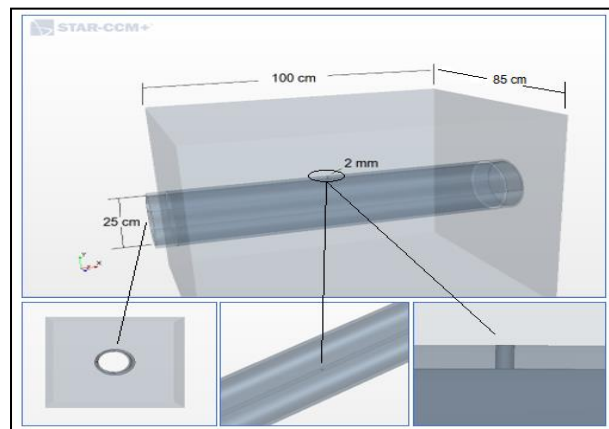


**Figure 5-3: Isometric view of pipeline geometry for CFD model using STAR-CCM software**

The boundary conditions of the developed CFD model are summarized below in Table 5-1, including the fluid's properties for single-phase and multi-phase flows. These have been considered from the previous hydrodynamic model as boundary conditions for the CFD model.

**Table 5-1: Boundary conditions and the fluid parameters for the CFD STAR-CCM simulation model**

Boundary Conditions /Fluid Properties	Single-phase/ Water	Multi-phase/ Gas Condensate
Simulation Type	3D- Turbulent	3D- Turbulent
Model	k-ε model	k-ε model
Inlet	velocity inlet	velocity inlet
Outlet	Pressure outlet	Pressure outlet
Wall	No-slip	No-slip
Inlet Temp. (°C)	16	12
Ocean Temp. (°C)	4.0	4.0
Density (kg/m <sup>3</sup> )	998.3167	352.4468
Velocity (m/sec)	9	9.5
Pipe Length (m)	1.0	1.0
Leak Sizes (mm)	0, 2, 4, 6, 8, 10, 12 and 14	2, 6, 10 and 14
Leak Position (m) (x, y, z)	(0.5, 0.25, 0)	(0.5, 0.25, 0)
Pipe ID /Length (m)	0.25/1	0.25/1
Viscosity (kg/sec-m)	0.0017	3.562E-05
Flow Rate (kg/sec)	192.8	495.2
Ambient Leak Pressure (psia)	160.0	160.0

The CFD model employs a finite volume method to numerically compute the partial differential equations, wherein the continuous function is solved at the discrete elements called mesh elements. It is recommended that the mesh near the walls and leak hole needs to be fine enough to resolve the small eddies elements, as shown in Figure 5-4 below. No slip boundary condition i.e.  $v=0$  is applied. The inlet boundary condition is set as a velocity inlet as detailed for each single-phase and multi-phase flow. The outlet boundary condition is set as the pressure outlet. The leak hole is also set as the pressure outlet. Thus, the leak outlet releases fluid into the water and the pressure outlet boundary at the leak orifice is assumed to be equal to 100 m of the water column ( $P_L = 160$  psi  $V_{water} = 0.1$  m/s). The temperature of the fluid inside the pipe is set at 16°C for single-phase flow

and 12°C for multi-phase flow, to match the simulated hydrodynamic model boundary conditions. The ambient temperature is set at 4°C, which is considered as the average temperature of the ocean water.

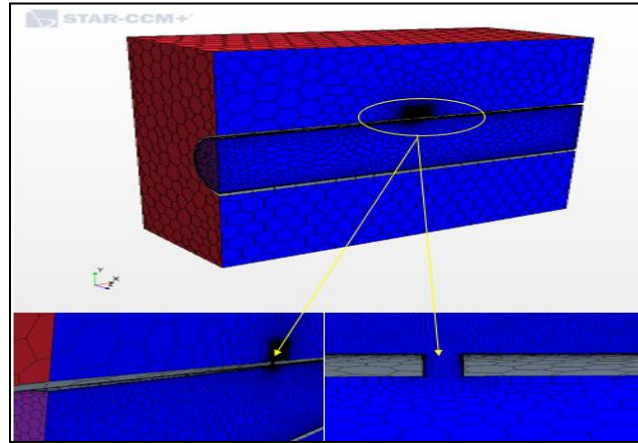


**Figure 5-4: Refined meshing of the pipeline at the near wall and leak hole**

PVT data describing the fluid’s compositional properties are developed by Akpabio et al. [61]. Other PVT data obtained for the gas condensate have been presented by Saleh and Stewart [60]. The approach is assumed to be an equation of a state compositional model to generate these Volumes of Fraction (VOF) values from PVT properties presented earlier in Table 4-2 above. The VOFs for multi-phase are calculated as: vapour is 0.9958 and liquid is 0.0042, shown in Table 5-2. The results of the pressure and temperature response to VOF variation have also been discussed below.

**Table 5-2: The volume of fraction (VOF) for gas condensate composition**

Gas Condensate	VOF/ Mole fraction	Vapour Phase	Liquid Phase
<b>Total</b>	<b>1</b>	<b>0.9958</b>	<b>0.0042</b>
Methane (C4H)	0.9050	0.9048	0.0000
Ethane (C2H6)	0.0500	0.0502	0.0000
Carbone Dioxide (CO2)	0.0301	0.0301	0.0001
Butane (C4H10)	0.0100	0.0105	0.0000
Water (H2O)	0.0040	0.0002	0.0010
Methanol (C4H4O)	0.0010	0.0007	0.0031

The CFD model simulates the fluid flow inclusively inside and outside the pipeline passing through a small leak to the ocean water. The adjacent ocean water is flowing and assumed to be moving in the same direction as inside the pipeline. After the CFD model is created, the model is validated to check the reliability of the model's performance. The validation criteria deployed in this work are based on past works that are used to compare the CFD models with the same boundary conditions. The validation steps for the proposed model are discussed below in the next section. Furthermore, different leak sizes and fluid types are used to examine the local temperature changes along the pipeline. In the last step of the first simulation methodology, a temperature change sensitivity analysis for DTS technology is developed from the model's temperature profile as shown in the results below. Finally, these analyses can be suggested to select the optimal LDS based DTS for a pipeline operator.

## **5.4 CFD Simulation Result**

### **5.4.1 Model Validation**

To validate the 3D CFD model, mass flow rate analysis is conducted for the steady-state condition to study the effect of pressure on the leak flow rate at the leak sizes of 2 and 10 mm. The developed model has been validated against the results reported in the literature by Ben-Mansour [36]. In Ben-Mansour [36], a CFD model is developed to simulate the effect of small leaks in water pipelines. The study is conducted using a 2 m long pipe and has an outside diameter of 0.1 m, with a uniformly shaped leak hole in the top-middle section of the pipeline. The fluid velocity is 1 m/s and line pressure readings are between 1- 6 bar for different leak sizes. The developed model is simulated for the

same conditions and checked to confirm the validity of this work. The leak flow rate is the factor of this validation process. The leak flow rate is observed at 10 and 2 mm leak sizes at the same pressure to show the leak flow rate performance. Results, shown in Figure 5-5 below, demonstrate a good match between the results of this study and the results reported in Ben-Mansour [36] and fall in the 5% of the error bars.

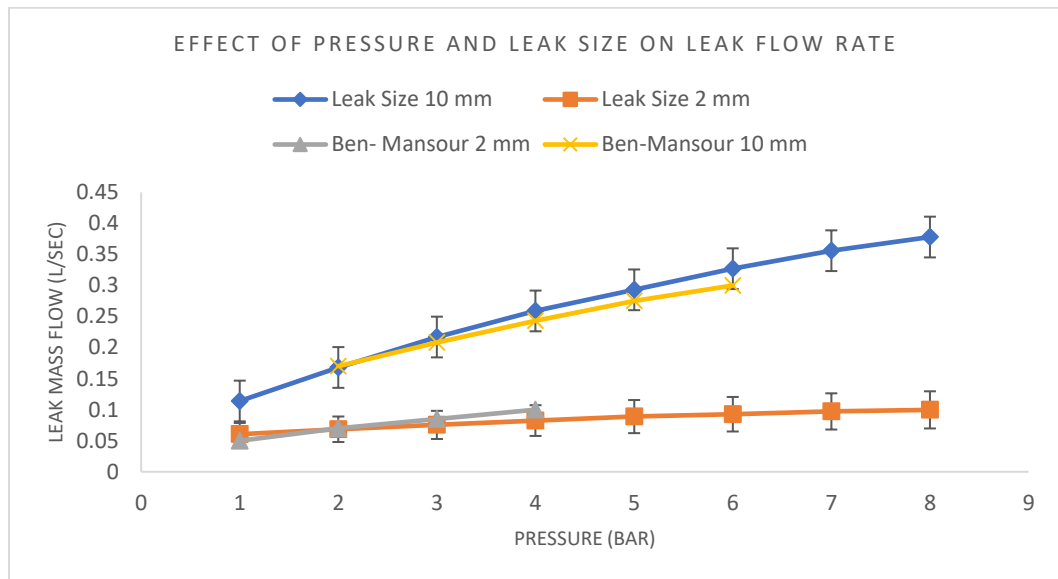


**Figure 5-5: CFD model validation with Ben-Mansour’s work (pipe length 2 m, leak sizes 2mm &10 mm, velocity 1 m/s, pressure 1 bar) [36]**

The CFD model thermal result is compared with another experimental study that was performed by Siebenaler et al. [40]. In the study, a series of tests were performed to determine if substantial thermal fields could result from underwater leaks. The tests were executed between 100 psi and 500 psi with 1/16-inch and 3/16-inch orifices. In addition, the study tested two fluid types (oil and water) separately. The study concluded that simulated leaks into underwater environments created highly turbulent jets in the near-field, which causes the reduction of thermal gradients ( $\Delta T$ ). In the current study, the thermal gradients of the leak column on top of the leak outlet to the seawater are

predicted for the same leak sizes that have been used in the others work, 1.58 mm (1/16”), 3.17 mm (1/8”), 4.76 mm (3/16”) and 6.35 mm (1/4”). Pressure is set to 50, 100, 200 psi; temperatures’ measurements are set to be the same as their experiment settings and recorded at a distance of 152.4 mm (6”) from the leak orifice.

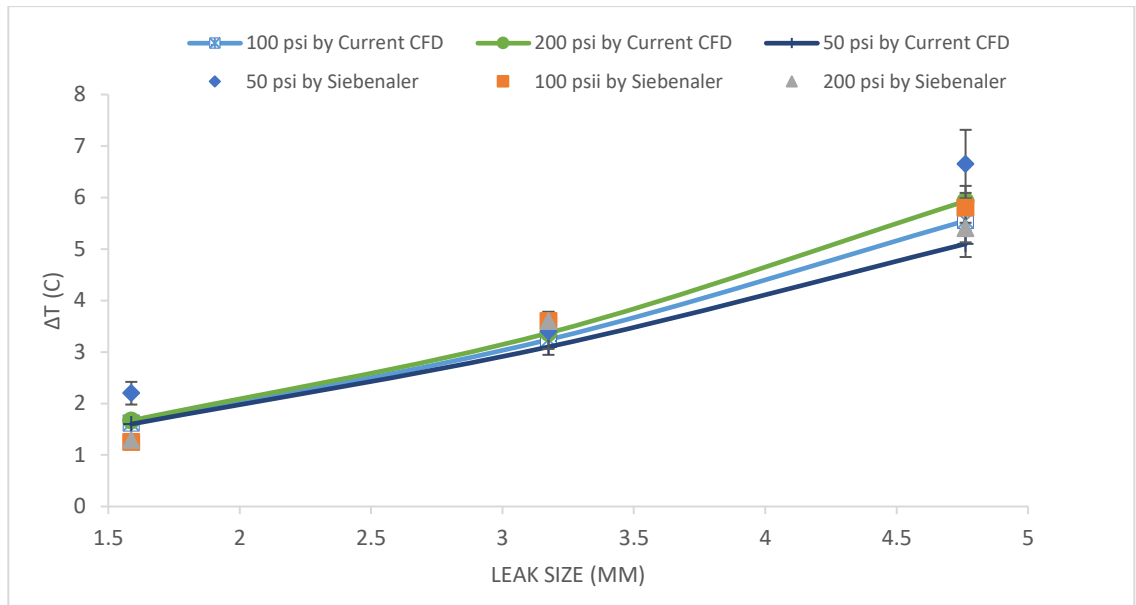


**Figure 5-6: CFD model validation of temperature changes  $\Delta T$  with leak sizes increase, compared with experimental jet-plume thermal gradient for liquid leaks, by Siebenaler et al. [40]**

As shown in Figure 5-6, the results from the current CFD demonstrated close matches to the results presented by Siebenaler et al [40] and fall in the 5% of the error bars. This suggests that the CFD model calculations can be used as reasonable approximations for future predictions.

#### 5.4.2 Transient Simulation for Leak Behaviour Characterization

Since it is relatively hard to detect the leak characteristics due to low fluid flow velocity using steady state information, a transient condition is developed for further pressure and

temperature profiles analysis around the leak orifice. Flow velocity inside the pipe was predicted from the hydrodynamic model as to 9 m/s for single-phase flow and 9.5 m/s for multi-phase flow, for a 1 m long and 0.25 m diameter (inner) pipe. The k- $\epsilon$  model has been used to model the turbulence. Single-phase flow and multi-phase flow are examined to observe the multi-phase flow effect on the pressure and temperature profiles. A leak can produce an instant change in the pressure and temperature profiles. The CFD model can calculate the parameters' changes along the outer surface of the pipe walls by creating a constrained line in the model geometry, located on top of the middle of the pipe. The line is used to calculate model parameters (i.e. pressure, temperature, etc.) according to the desired information. For example, the pressure profile obtained along the constrained line varied close to the leak orifice due to a leak jet and peaked to the highest value at the top of the leak nozzle. The leak sizes were considered in the simulation for single-phase flow case; 2, 4, 6, 8, 10, and 12 mm. Each of these leak sizes was tested in the CFD model individually to calculate the needed pressure and temperature profiles. Then, all these results were summarized in one chart as shown in Figure 5-7.

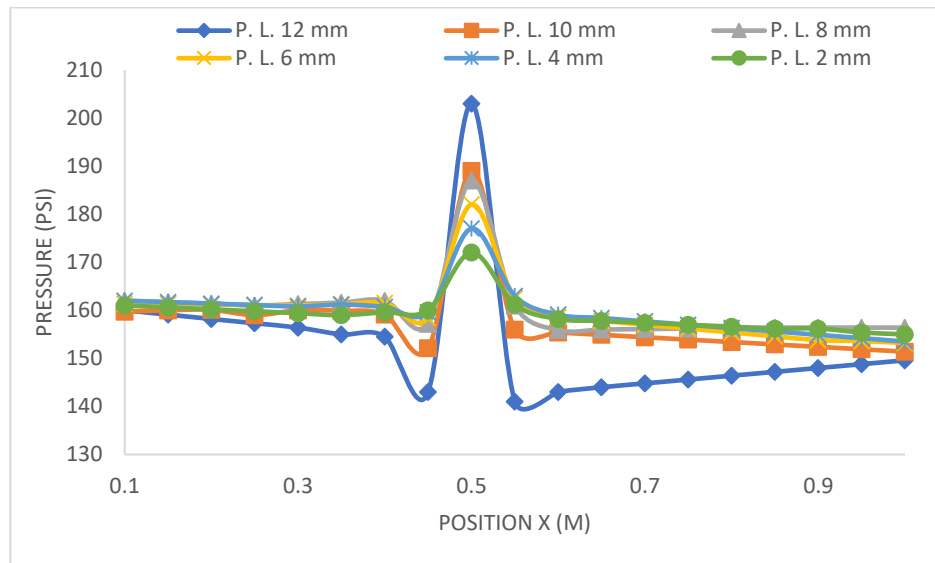


**Figure 5-7: Pressure profile for single-phase flow case, along the pipe’s outer wall for leak sizes from 2 to 14 mm at 0.5 m from the inlet**

Multi-phase flow is believed to have a different mechanism than single-phase flow for pressures and temperatures profiles. Results from the single-phase flow case were compared with the results of the multi-phase flow case to demonstrate a better understanding of that belief. The multi-phase flow effect on pressure profile is shown for the leak sizes of 2 mm and 10 mm in Figure 5-8. Hence, the pressure profile results comparison can demonstrate the influence due to multi-phase flow. For example, in the single-phase flow case, the pressure fluctuates from 150 to 170 psi for the 2 mm leak and then from 150 to 185 psi for the 10 mm leak. In contrast, for the same leak sizes in the case of a multi-phase flow, the pressure fluctuates from 160 to 162 psi for the 2 mm leak and then from 160 to 166 psi for the 10 mm leak. Because of the flow turbulence has affected the multi-phase flow; the single-phase flow has a higher pressure effect on the surroundings than the multi-phase flow dose.

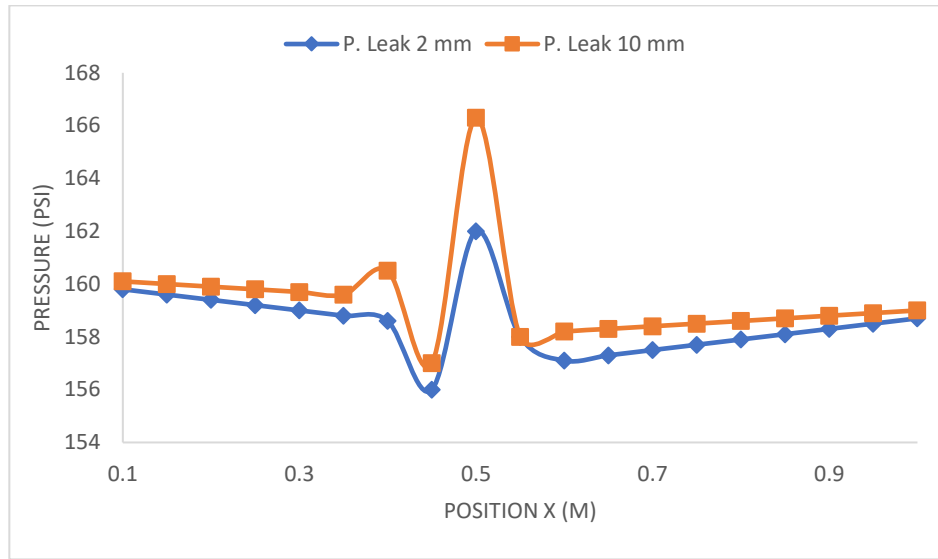


**Figure 5-8: Pressure profile for multi-phase flow case, along the pipe’s outer wall for leak sizes from 2 to 14 mm at 0.5 m from the inlet**

### 5.4.3 Volume of Fraction Effect on Temperature Profiles

The CFD model is used to examine the VOF effect on pressure and temperature around the leak hole (2 mm) in the pipe. The PVT file covering the fluid’s compositional properties has been presented earlier in Table 5-3. That PVT data is used to generate the VOF using PVTSIM software. In this analysis, the considered VOF of the vapour and liquid phases for the condensate (1, 2, and 3) compositions are shown in Table 5-3.

**Table 5-3: Volume of fraction (VOF) of vapour and liquid phases, for condensates (1, 2, and 3)**

Condensate	VOF	Vapour fraction	Liquid fraction
Condensate 1	VOF 1	0.8181	0.1819
Condensate 2	VOF 2	0.7949	0.2051
Condensate 3	VOF 3	0.7759	0.2241

The sensitivity of temperature to the VOF around the leak is developed for the three condensate mixtures. As a result, the temperature profiles showed a sensible VOF effect according to the different compositional condensates (1, 2, and 3) with about 0.1 °C difference between each of them, as shown in Figure 5-9.

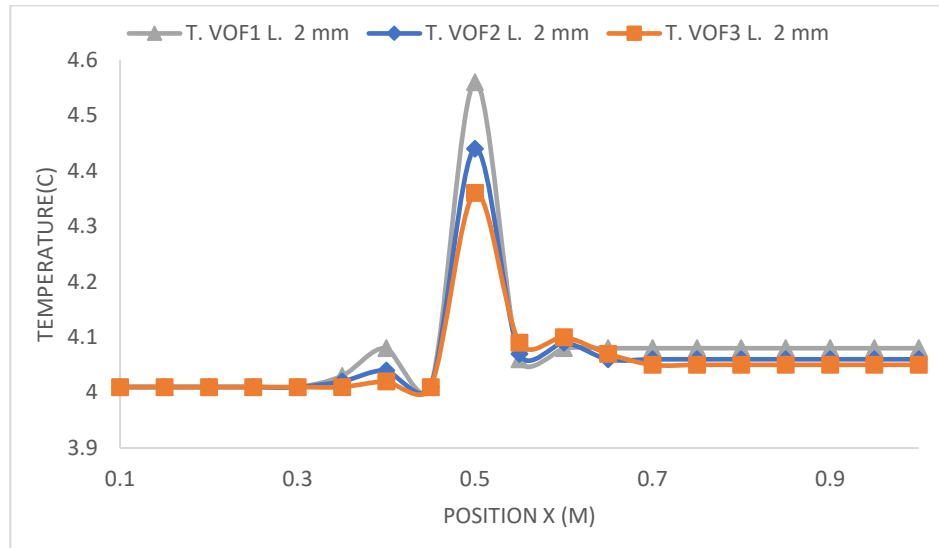


**Figure 5-9: Temperature Profile for Condensates 1, 2 and 3, along the pipe's outer surface with 2 mm leak size**

#### **5.4.4 Leak Size Sensitivity Analysis on Temperature Profiles**

The developed CFD model results demonstrate an accommodating technique to illustrate the effect of leak size on the temperature change  $\Delta T$  ( $T_{leak} - T_{ambient}$ ) around the leak hole. The leak size impact on the temperature change around the leak is one of the most significant factors to determine the temperature sensitivity for the LDS based DTS. The leak size increase can influence the fluid thermal gradient through the leak orifice to the cold sea water. In the case of the single-phase flow, the leak sizes considered in the simulation are 0, 2, 4, 6, 8, 10, 12 and 14 mm. The temperature changes calculations along the measuring line were stable at 4 °C for the entire distance from the pipe inlet until peaking at the point where the leak exists and then falling again to 4 °C. The leak size (0 mm) proved that no leak existed, as there was no change in the temperature profile along the wall outer surface. The other leak sizes showed sensible increases in the temperature change around the leak hole. The measuring line was created on top of the pipe section in the model's geometry parts at 0.01 mm from the wall's outer surface. The

measuring line can act to sense the temperature similarly to the installed FOC along the subsea pipeline. As the leak size increased, the temperature change ( $\Delta T_{leak}$ ) around the leak hole increased. The temperature sensitivity for different leak sizes in the case of the single-phase flow is shown in Figure 5-10.

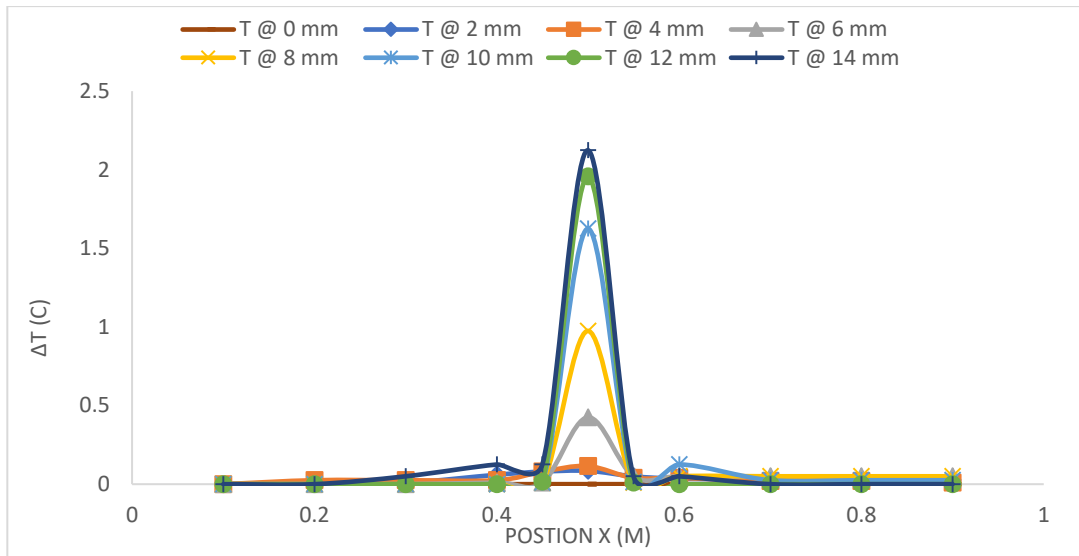


**Figure 5-10: Temperature profiles for single phase flow case, along the pipe's outer surface for leak sizes from 0 to 14 mm at 0.5 m distance from the pipe inlet**

In the case of the multi-phase flow, the temperature profiles were developed for leak sizes of 2, 6, 10 and 14 mm, as shown in Figure 5-11. There is a significant difference between the prior single-phase flow temperature profile results and the multi-phase flow case. In fact, the multi-phase flow case has influenced the temperature change ( $\Delta T_{leak}$ ) and showing less increase as the leak size increases. For example, at a leak size of 10 mm, the temperature change ( $\Delta T_{leak}$ ) increased at the leak orifice (0.5 m distance from the inlet) and recorded a 1.5 °C in the single-phase flow case. In contrast, at the same leak size, the temperature change ( $\Delta T_{leak}$ ) reached to only a 0.1 °C in the multi-phase

flow case. This is relatively due to the flow turbulence has influenced the multi-phase flow thermal behaviour.

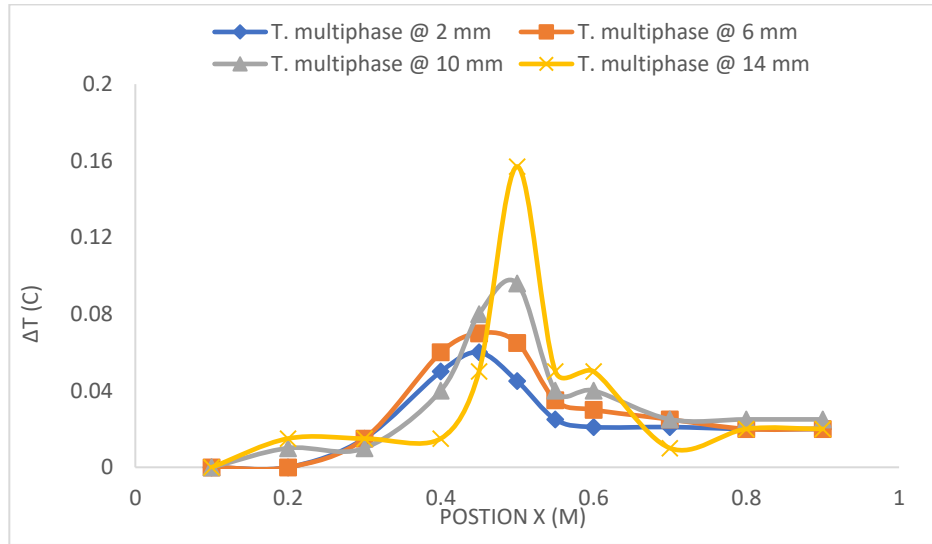


**Figure 5-11: Temperature profiles for multi-phase flow case, along the pipe’s outer surface for leak sizes from 2 to 14 mm at 0.5 m distance from the pipe inlet**

In addition, 2D colored contours present the temperature around the leak orifice and show the effect of different leak sizes on the temperature range near the leak hole. In the single-phase flow, the range of the temperature contours increases as leak size increases. Leak sizes of 2, 4, 6, and 8 mm are presented, as shown in Figures 5-12 and 5-13. Also, the charts show ocean water movement affects the contour’s shape in same water flow direction.

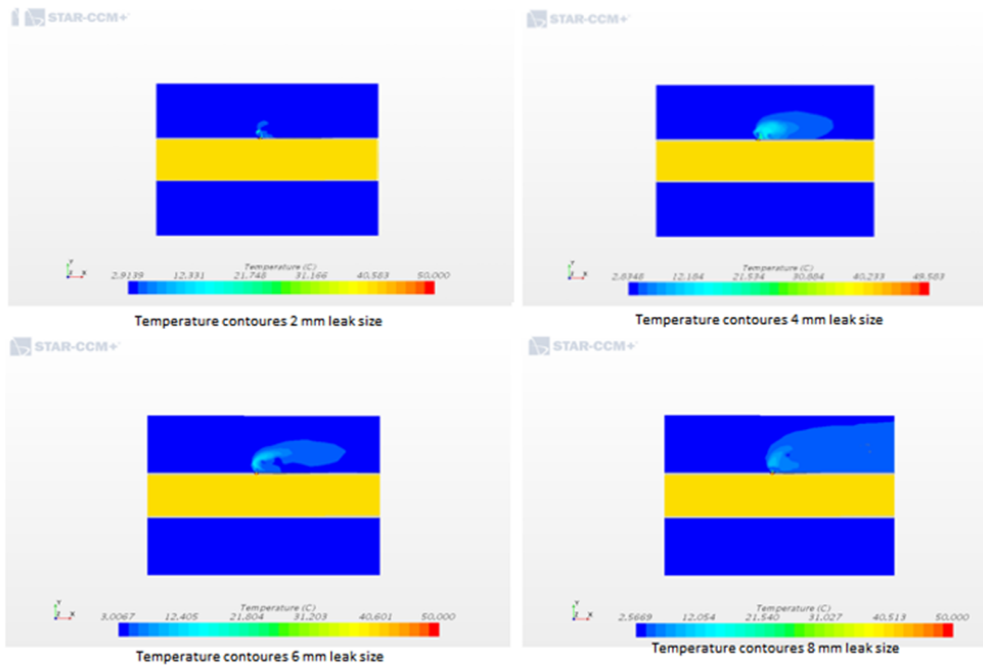


Figure 5-12: Temperature contours around the leak in single-phase flow for leak sizes from 2 to 8 mm at 0.5 m from the inlet

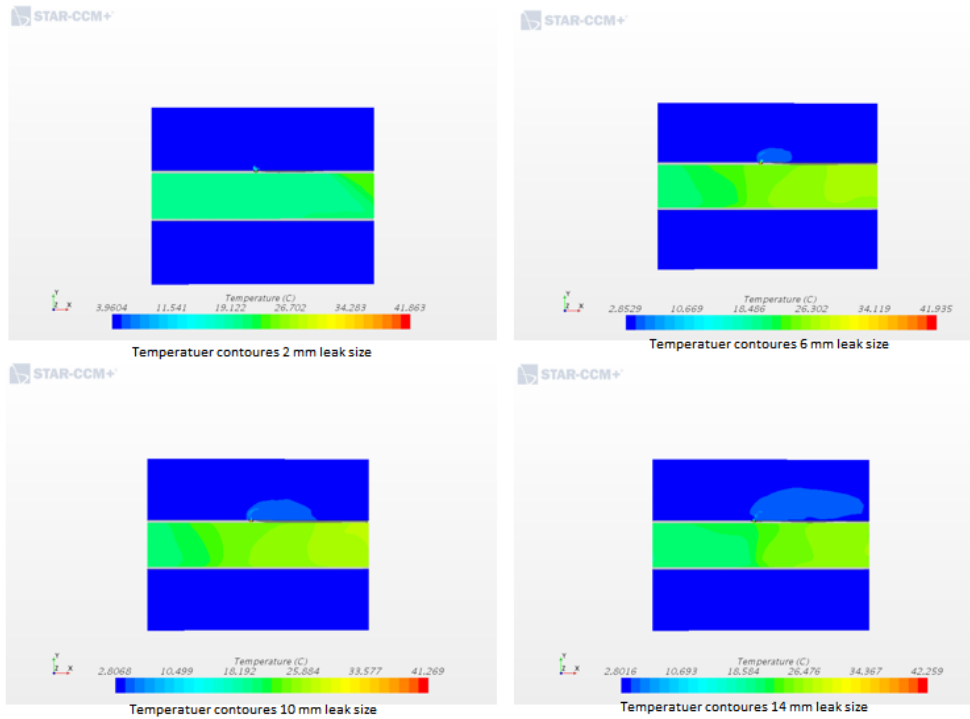
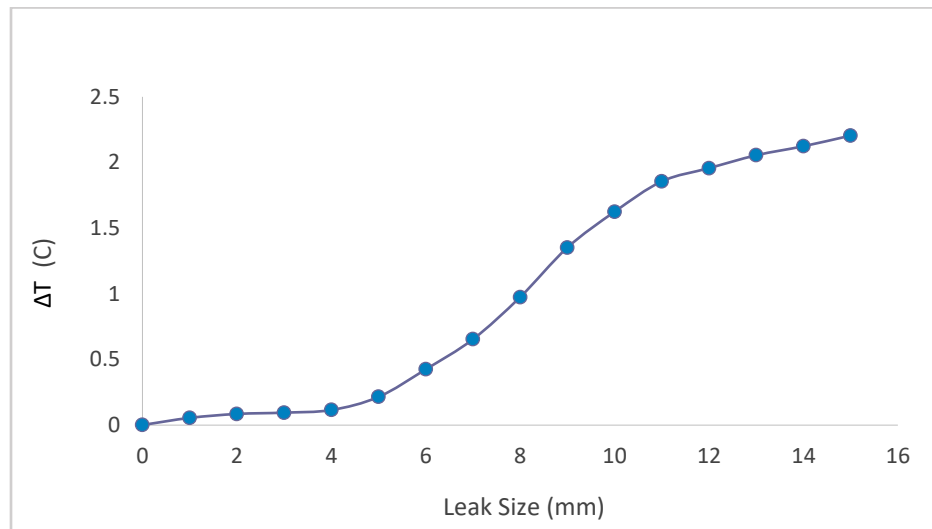
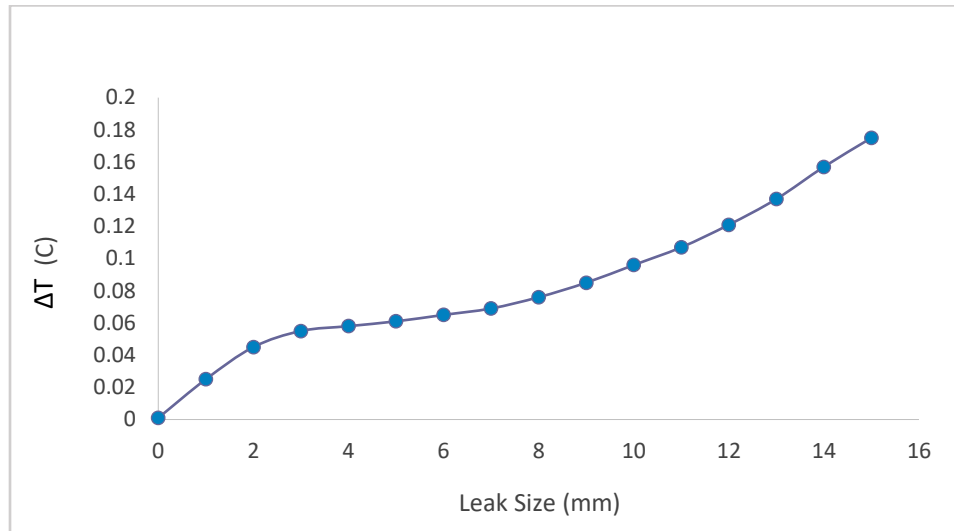


Figure 5-13: Temperature contours around the leak in multi-phase flow for leak sizes from 2 to 14 mm at 0.5 m from the inlet

The temperature change ( $\Delta T$ ) around the leak increased as the leak size has increased. This is simply because for larger leak more mass at elevated temperature is released to the environment at any given time which causes the rise in surrounding temperature. The charts in Figure 5-14 and 5-15 are shown the temperature sensitivity for a probable leak size at each of phase flow condition. The multi-phase flow case showed temperature changes  $\Delta T$  on top of the leak hole have a much influence on the fluid type and flow conditions than the single-phase case does. The temperature change  $\Delta T$  ( $^{\circ}\text{C}$ ) is predicted to model temperature sensitivity for each millimeter increment in leak diameter.



**Figure 5-14: Sensitivity chart of leak size effect on  $\Delta T$  for single-phase flow at 0.5 m from the inlet**



**Figure 5-15: Sensitivity chart of leak size effect on  $\Delta T$  for multi-phase flow at 0.5 m from the inlet**

The temperature change  $\Delta T$  ( $^{\circ}\text{C}$ ) is predicted to model the temperature sensitivity in case of developing a DTS technology project. The thermal gradient of the leak column on top of the leak outlet to the sea water is predicted for different leak sizes as shown in Figure 5-16. The graph shows the temperature sensitivities at leak sizes of 0, 2, 4, 6, 8, 10, 12 and 14 mm. In this case, CFD model used the water as fluid type in the single-phase flow condition and at constant pressure and flow rate. Possible small leaks that impose directly contact to the pipeline surroundings can produce significant near field temperature changes that may be measurable by temperature-based technologies such as DTS. The leak column transition on top of the leak versus the thermal gradient sensitivity ( $\Delta T$ ) graph that shown in Figure 5-16 can help pipeline operators to choose the optimal LDS design parameters for fiber optic technology based DTS.

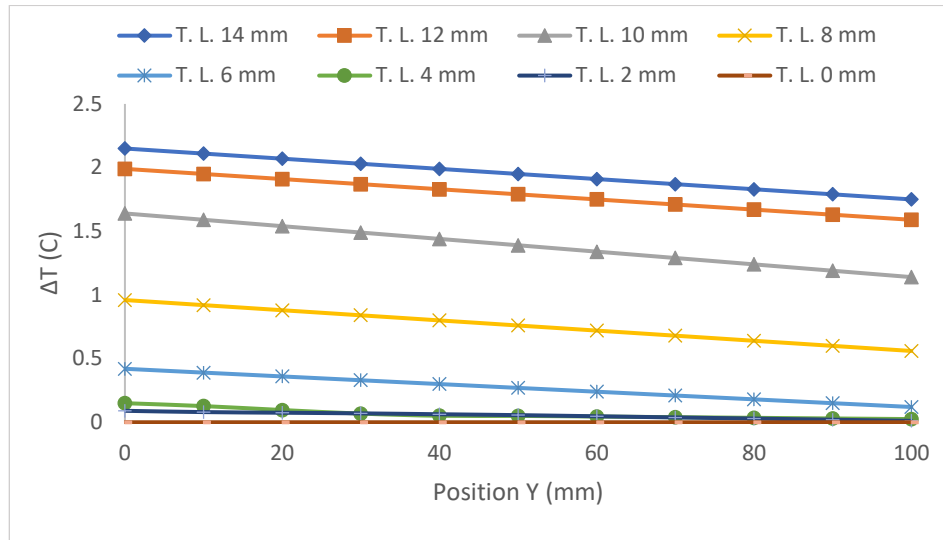


**Figure 5-16: Temperature vertical range on top of pipe leak for single-phase flow**

Similarly, Figure 5-17, for the multi-phase flow case is presented using the temperature profile results at leak sizes of 2, 6, 10 and 14 mm. The thermal gradient of the leak column on top of the leak outlet to the seawater showed deferent presentation in case of the multi-phase flow.

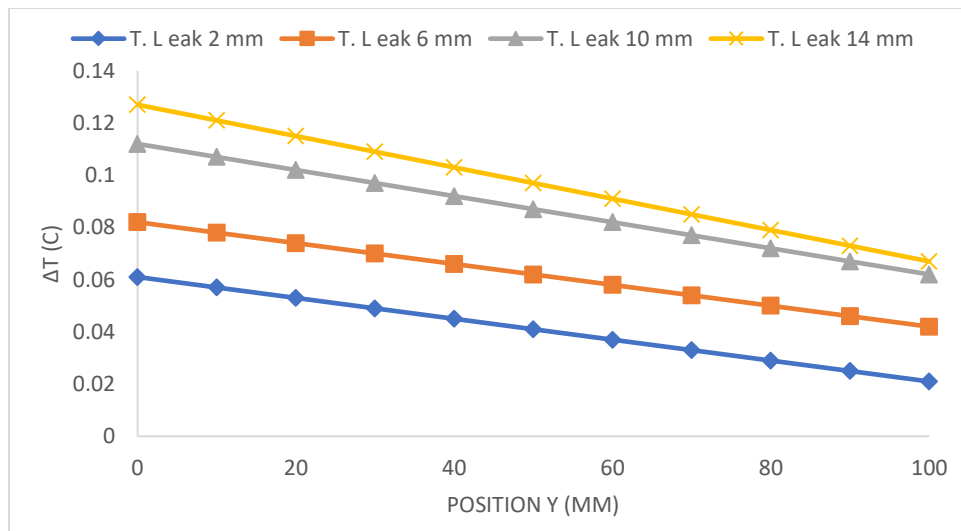


**Figure 5-17: Temperature vertical range on top of pipe leak for multi-phase flow**

According to Kumar and Nigam [62], the multi-phase flow has a slightly different presentation from the single-phase flow. The present analysis shows an agreement with this published work; the temperature change ( $\Delta T_{leak}$ ) on top of the leak outlet in the multi-phase flow case showed a different presentation from the single-phase flow case for the same leak sizes. The single-phase fluid is denser than the multi-phase composition, which might be a reason for this variation. In another study, Siebenaler et al. [40] asserted that the simulated leaks into underwater environments created highly turbulent jets in the surroundings, which resulted in a reduction of thermal gradients. Their findings agree with the current study temperature change analyses, where the thermal gradient ( $\Delta T_{leak}$ ) of the leaked fluid column on top of the leak outlet diminishes as it moves further away from the pipeline. In fact, possible small leaks that directly contact the pipeline's surroundings can produce significant near field temperature changes that may be measurable by temperature-based technologies such as DTS. The thermal gradient sensitivity ( $\Delta T_{leak}$ ) in Figures 5-16 and 5-17 can help pipeline operators to choose the optimal LDS design parameters when they develop an LDS based DTS technology project.

## **Chapter 6: Conclusions and Recommendations**

### **6.1 Summary and Conclusions**

The first part of this thesis is aimed to develop a hydrodynamic model to determine the segment of the pipeline system in most critical condition. The hydrodynamic model of 150 km pipeline length has been developed using AFT software to examine the temperature and pressure profiles along the pipeline. The most extreme condition is observed at 30 km from the pipeline inlet. A pipe segment at this distance and with these conditions is suggested for the second part of sophisticated CFD simulation using the STAR-CCM software. Therefore, CFD transient simulations for both single-phase and multi-phase flow have been conducted using a 3D turbulent model to determine the effect of the leak size on the surrounding pressure and temperature profiles. The temperature profile outcomes are used to analyze the effect of different leak sizes on the thermal gradient around the leak hole. Results show the leak size increase has increased the thermal gradient of the leaked fluid column on top of the leak outlet. The study outcomes are in good agreement with theoretical and past experimental findings. The single-phase flow and multi-phase flow simulations results presented the local pressure and temperature profiles for different leak sizes. The outcomes showed the pressure and temperature fluctuations are highly localized at the top pipeline leakage zone, the thermal gradient ( $\Delta T_{\text{leak}}$ ) of the leaked fluid column on top of the leak outlet diminishes as it moves further away from the pipeline's outer wall. However, the multi-phase flow has influenced the pressure and temperature profiles' presentation through the ocean water under the same conditions and leak sizes. This can be seen from the simulation results

for the temperature change around the leak hole as increased with the variation of the vapour to liquid fractions. Similarly, the effect of VOF variation in a multi-phase flow is also affected the pressure profile results. This study helps to understand the leak's effect on the surrounding environment. Pipeline operators can use the results for determining the specifications needed to design the most appropriate LDS for the pipelines, especially with Fibre Optic Leak Detection Systems based DTS technology.

The main contribution of this thesis is the development of a methodology to study the leak in the subsea pipeline and its surrounding environment combining hydrodynamic model and CFD model. The use of hydrodynamic model allows studying long pipelines without any significant increase of computational burden.

The other contributions of the study are:

- Selection of the most critical segment in a long pipeline which can be subsequently studied using a sophisticated CFD simulation based on the most extreme condition.
- The hydrodynamic model provided the boundary conditions for the CFD model.
- A CFD model of a pipeline section with a leak at the top is developed to predict the pressure and temperature profiles around the pipe's leak surroundings.
- A single-phase flow simulation is presented to observe the local pressure and temperature changes for different leak sizes. Results showed the pressure and temperature fluctuations are highly localized at the top pipeline leakage zone.

- A multi-phase flow simulation is presented to observe the local pressure and temperature changes for different leak sizes. However, results showed that the multi-phase flow has influenced the temperature changes around the leak ( $\Delta T_{leak}$ ), and showing less increase than the single-phase flow for the same leak sizes with other conditions.
- Effect of VOF variation in multi-phase flow has been examined. Results showed that there is a noticeable difference in the temperature fluctuations at the top pipeline leakage zone if VOF is changed.
- Effect of different leak sizes on temperature sensitivity around the leak hole has been studied. Sensitivity analyses of the temperature and leak sizes for both single-phase and multi-phase flow have been presented. Results demonstrated in the multi-phase flow show a significant influence on the temperature change around the leak hole.

## 6.2 Recommendations

Knowing the importance of LDSs in the prevention of economic and environmental impacts led pipeline operators to seek for more detailed understanding of the leak's behaviour to determine the best possible technology available. This study simulates the fluid flow from inside the pipeline leaking into the unsteady ocean water in one computational environment. Pipeline leaks simulations using CFD approach will assist pipeline operators to design the optimal LDS for their pipeline system. Advanced technologies such as DTS, are preferred to provide real-time leak detection coverage over the long length of pipelines. In the current work, the sensitivity analyses of

temperature changes around the leak hole are proposed to understand a leak's effect on the surrounding water and the pipeline's outer wall. For example, these analyses can be suggested to find the needed spatial resolution to design Fiber Optic Cable Distributed Sensing Solutions based DTS technology.

### **6.3 Future work**

The turbulent models have been studied to determine the influence of leak size on the critical parameters (i.e. pressure and temperature) for single-phase and multi-phase flow conditions. However, there is a chance of hydrate formation for low temperature and high-pressure conditions near the leakage which is not considered in the study. Hereafter, this critical concern should be considered.

## Bibliography

- [1] G. E. Schweitzer, *Countering Terrorism: Biological Agents, Transportation Networks, and Energy Systems: Summary of a US-Russian Workshop*. 2009.
- [2] S. L. Scott and M. A. Barrufet, *Worldwide Assessment of Industry Leak Detection Capabilities for Single & Multiphase Pipelines*. 2003.
- [3] P. Murvay and I. Silea, "A survey on gas leak detection and localization techniques," *J Loss Prev Process Ind*, vol. 25, (6), pp. 966-973, 2012.
- [4] P. Thodi *et al*, "Arctic pipeline leak detection using fiber optic cable distributed sensing systems," in *OTC Arctic Technology Conference*, 2014.
- [5] L. J. Li *et al*, "Overview of fiber optic pipeline monitoring sensors," in *Applied Mechanics and Materials*, 2013.
- [6] B. Eisler and G. A. Lanan, "Fiber optic leak detection systems for subsea pipelines," in *Offshore Technology Conference*, 2012.
- [7] A. Mishra and A. Soni, "Leakage detection using fibre optics distributed temperature sensing," in *6th Pipeline Technology Conference*, 2011.
- [8] H. Versteeg and W. Malalasekera, "Computational fluid dynamics," *The Finite Volume Method*, 1995.
- [9] J. D. Anderson and J. Wendt, *Computational Fluid Dynamics*. 1995206.

- [10] J. H. Ferziger and M. Peric, *Computational Methods for Fluid Dynamics*. 2012.
- [11] D. C. Wilcox, *Turbulence Modeling for CFD*. 19982.
- [12] N. Turner, "Hardware and software techniques for pipeline integrity and leak detection monitoring," in *Offshore Europe*, 1991.
- [13] J. Zhang, "Designing a cost-effective and reliable pipeline leak-detection system," *Pipes Pipelines Int.*, vol. 42, (1), pp. 20-26, 1997.
- [14] A. S. Willsky, "A survey of design methods for failure detection in dynamic systems," *Automatica*, vol. 12, (6), pp. 601-611, 1976.
- [15] H. Brones and H. Schaffhaussen, "European methods of leak detection and location," *Pipeline Industry*, pp. 50-66, 1972.
- [16] R. Isermann and B. Freyermuth, "Process Fault Diagnosis Based on Process Model Knowledge: Part I—Principles for Fault Diagnosis With Parameter Estimation," *Journal of Dynamic Systems, Measurement, and Control*, vol. 113, (4), pp. 620-626, 1991.
- [17] R. Isermann, "Model-based fault diagnosis of technical systems- Approach principles and examples," *Zeitschrift Fuer Flugwissenschaften Und Weltraumforschung*, vol. 20, (1), pp. 1-17, 1996.
- [18] L. Billmann and R. Isermann, "Leak detection methods for pipelines," *Automatica*, vol. 23, (3), pp. 381-385, 1987.

- [19] R. Isermann, "Process fault detection based on modeling and estimation methods—A survey," *Automatica*, vol. 20, (4), pp. 387-404, 1984.
- [20] R. Isermann, "Process fault diagnosis with parameter estimation methods," in *Digital Computer Applications to Process Control* Anonymous 1986.
- [21] G. Wang, D. Dong and C. Fang, "Leak detection for transport pipelines based on autoregressive modeling," *IEEE Transactions on Instrumentation and Measurement*, vol. 42, (1), pp. 68-71, 1993.
- [22] J. C. Liou and J. Tian, "Leak detection—transient flow simulation approaches," *Journal of Energy Resources Technology*, vol. 117, (3), pp. 243-248, 1995.
- [23] K. A. Loparo, M. Buchner and K. S. Vasudeva, "Leak detection in an experimental heat exchanger process: a multiple model approach," *IEEE Transactions on Automatic Control*, vol. 36, (2), pp. 167-177, 1991.
- [24] N. Y. Lee, I. S. Hwang and H. Yoo, "New leak detection technique using ceramic humidity sensor for water reactors," *Nucl. Eng. Des.*, vol. 205, (1-2), pp. 23-33, 2001.
- [25] M. Ferrante and B. Brunone, "Pipe system diagnosis and leak detection by unsteady-state tests. 1. Harmonic analysis," *Adv. Water Resour.*, vol. 26, (1), pp. 95-105, 2003.
- [26] S. Hyun *et al*, "An experimental study on a ground-penetrating radar for detecting water-leaks in buried water transfer pipes," in *Antennas, Propagation and EM Theory, 2003. Proceedings. 2003 6th International Symposium On*, 2003.

- [27] S. R. Mounce *et al*, "Sensor-fusion of hydraulic data for burst detection and location in a treated water distribution system," *Information Fusion*, vol. 4, (3), pp. 217-229, 2003.
- [28] D. Kurtz, "Pure Technologies US Inc," *Central Regional Office*, vol. 7107, 2006.
- [29] B. Mergelas and G. Henrich, "Leak locating method for pre-commissioned transmission pipelines," *North American Case Studies*, 2005.
- [30] Y. Gao *et al*, "On the selection of acoustic/vibration sensors for leak detection in plastic water pipes," *J. Sound Vibrat.*, vol. 283, (3-5), pp. 927-941, 2005.
- [31] Y. Gao, M. Brennan and P. Joseph, "A comparison of time delay estimators for the detection of leak noise signals in plastic water distribution pipes," *J. Sound Vibrat.*, vol. 292, (3-5), pp. 552-570, 2006.
- [32] M. Brennan, Y. Gao and P. Joseph, "On the relationship between time and frequency domain methods in time delay estimation for leak detection in water distribution pipes," *J. Sound Vibrat.*, vol. 304, (1-2), pp. 213-223, 2007.
- [33] C. Verde, N. Visairo and S. Gentil, "Two leaks isolation in a pipeline by transient response," *Adv. Water Resour.*, vol. 30, (8), pp. 1711-1721, 2007.
- [34] S. Hiroki *et al*, "Development of water leak detection method in fusion reactors using water-soluble gas," *Fusion Eng. Des.*, vol. 83, (1), pp. 72-78, 2008.

- [35] J. Yang, Y. Wen and P. Li, "Leak location using blind system identification in water distribution pipelines," *J. Sound Vibrat.*, vol. 310, (1-2), pp. 134-148, 2008.
- [36] R. Ben-Mansour *et al*, "Computational fluid dynamic simulation of small leaks in water pipelines for direct leak pressure transduction," *Comput. Fluids*, vol. 57, pp. 110-123, 2012.
- [37] M. de Vasconcellos Araújo *et al*, "Numerical study of oil flow in tee junction with leaks," *Advances in Petroleum Exploration and Development*, vol. 6, (2), pp. 1-11, 2013.
- [38] H. Zhu, P. Lin and Q. Pan, "A CFD (computational fluid dynamic) simulation for oil leakage from damaged submarine pipeline," *Energy*, vol. 64, pp. 887-899, 2014.
- [39] S. Cloete, J. E. Olsen and P. Skjetne, "CFD modeling of plume and free surface behaviour resulting from a sub-sea gas release," *Appl. Ocean Res.*, vol. 31, (3), pp. 220-225, 2009.
- [40] S. Siebenaler *et al*, "Thermal characterization of potential leaks in offshore pipelines," in *OTC Arctic Technology Conference*, 2015.
- [41] R. S. Reddy *et al*, "Pressure and flow variation in gas distribution pipeline for leak detection," in *Industrial Technology (ICIT), 2016 IEEE International Conference On*, 2016.
- [42] M. Jujuly *et al*, "Computational fluid dynamics modeling of subsea pipeline leaks in arctic conditions," in *Arctic Technology Conference*, 2016.

- [43] W. Liang *et al*, "Gas pipeline leakage detection based on acoustic technology," *Eng. Failure Anal.*, vol. 31, pp. 1-7, 2013.
- [44] S. C. De Schepper, G. J. Heynderickx and G. B. Marin, "CFD modeling of all gas–liquid and vapour–liquid flow regimes predicted by the Baker chart," *Chem. Eng. J.*, vol. 138, (1), pp. 349-357, 2008.
- [45] J. Dinis, A. Wojtanowicz and S. Scott, "Leak detection in liquid subsea flowlines with no recorded feed rate," *Transactions-American Society of Mechanical Engineers Journal of Energy Resources Technology*, vol. 121, pp. 161-166, 1999.
- [46] K. Afebu *et al*, "Integrated leak detection in gas pipelines using OLGA simulator and artificial neural networks," in *Abu Dhabi International Petroleum Exhibition and Conference*, 2015.
- [47] S. L. Scott and J. Yi, "Detection of critical flow leaks in deepwater gas flowlines," in *SPE Annual Technical Conference and Exhibition*, 1998.
- [48] T. Walters, "Gas-flow calculations: Don't choke," *Chemical Engineering*, vol. 107, (1), pp. 70-76, 2000.
- [49] B. Munson, D. Young and T. Okiishi, "Fundamentals of fluid mechanics," *Oceanographic Literature Review*, vol. 10, (42), pp. 831, 1995.
- [50] M. M. Zdravkovich, *Flow Around Circular Cylinders: Volume 2: Applications*. 1997.

- [51] B. Winters and T. Walters, "X-34 High Pressure Nitrogen Reaction Control System Design and Analysis," *Http://Www.Aft.Com*, 1997, Retrieved: Nov 12, 2017.
- [52] A. J. Osiadacz and M. Chaczykowski, "Comparison of isothermal and non-isothermal pipeline gas flow models," *Chem. Eng. J.*, vol. 81, (1-3), pp. 41-51, 2001.
- [53] D. G. Pavlou, *Composite Materials in Piping Applications: Design, Analysis and Optimization of Subsea and Onshore Pipelines from FRP Materials*. 2013.
- [54] A. Ghanbari, F. F. Fred and H. Rieke, "Newly developed friction factor correlation for pipe flow and flow assurance," *Journal of Chemical Engineering and Materials Science*, vol. 2, (6), pp. 83-86, 2011.
- [55] C. J. Chen, *Fundamentals of Turbulence Modelling*. 1997.
- [56] F. R. Menter, "Improved two-equation k-omega turbulence models for aerodynamic flows," 1992.
- [57] F. R. Menter, "Two-equation eddy-viscosity turbulence models for engineering applications," *Aiaa J.*, vol. 32, (8), pp. 1598-1605, 1994.
- [58] S. B. Pope, *Turbulent Flows*, 2001.
- [59] R. Tafreshi *et al*, "Two-phase heat transfer modeling in subsea pipelines," in *Integrated Systems: Innovations and Applications* Anonymous 2015.

[60] A. Saleh and G. Stewart, "Interpretation of gas condensate well tests with field examples," in *SPE Annual Technical Conference and Exhibition*, 1992.

[61] J. U. Akpabio, S. O. Isehunwa and O. O. Akinsete, "PVT Fluid Sampling, Characterization and Gas Condensate Reservoir Modeling," (*SCIENCEDOMAIN*), 2015.

[62] V. Kumar and K. Nigam, "Multiphase fluid flow and heat transfer characteristics in microchannels," *Chemical Engineering Science*, 2017.

# Appendices

## Appendix A: AFT Model's Data

### I. Single-Phase Flow Case

#### I.1 Input data single-phase flow case:

Pressure/Head Tolerance= 0.0001 relative change  
 Flow Rate Tolerance= 0.0001 relative change  
 Temperature Tolerance= 0.0001 relative change  
 Flow Relaxation= (Automatic)  
 Pressure Relaxation= (Automatic)  
 Heat Transfer with Energy Balance (with Constant Density)  
 Fluid Database: AFT Standard  
 Fluid: Water at 1 atm  
 Max Fluid Temperature Data= 212 deg. F  
 Min Fluid Temperature Data= 32 deg. F  
 Temperature= 0 deg. C  
 Density= 999.8884 kg/m<sup>3</sup>  
 Viscosity= 0.00177 kg/sec-m  
 Vapour Pressure= 0.00704 bar  
 Viscosity Model= Newtonian  
 Apply laminar and non-Newtonian correction to: Pipe Fittings & Losses, Junction K factors, Junction Special Losses, Junction Polynomials  
 Corrections applied to the following junctions: Branch, Reservoir, Assigned Flow, Assigned Pressure, Area Change, Bend, Tee or  
 Wye, Spray Discharge, Relief Valve  
 Ambient Pressure (constant)= 10 bar  
 Gravitational Acceleration= 1 g  
 Turbulent Flow Above Reynolds Number= 4000  
 Laminar Flow Below Reynolds Number= 2300

Table I: Pipes lengths/ sizes

Pipe	Name	Pipe Defined	Length	Length Units	Hydraulic Diameter	Hydraulic Diam. Units	Friction Data Set	Roughness	Roughness Units	Losses (K)	Initial Flow
1	Pipe	Yes	30	km	25.4508	cm	Standard	0.004572	cm	0	
2	Pipe	Yes	100	km	25.4508	cm	Standard	0.004572	cm	0	
3	Pipe	Yes	10	km	25.4508	cm	Standard	0.004572	cm	0	
4	Pipe	Yes	1	km	25.4508	cm	Standard	0.004572	cm	0	
Pipe	Initial Flow Units	Junctions (Up,Down)	Geometry	Material	Size	Type	Special Condition				
1		1, 3	Cylindrical Pipe	Steel - ANSI	10 inch	STD (s chedule 40)	None				
2		3, 4	Cylindrical Pipe	Steel - ANSI	10 inch	STD (s chedule 40)	None				
3		4, 6	Cylindrical Pipe	Steel - ANSI	10 inch	STD (s chedule 40)	None				
4		6, 5	Cylindrical Pipe	Steel - ANSI	10 inch	STD (s chedule 40)	None				

## I.2 Output data single-phase flow case:

Execution Time= 0.14 seconds  
 Total Number Of Head/Pressure Iterations= 0  
 Total Number Of Flow Iterations= 4  
 Total Number Of Temperature Iterations= 5  
 Number Of Pipes= 4  
 Number Of Junctions= 5  
 Matrix Method= Gaussian Elimination With Pivoting  
 Pressure/Head Tolerance= 0.0001 relative change  
 Flow Rate Tolerance= 0.0001 relative change  
 Temperature Tolerance= 0.0001 relative change  
 Flow Relaxation= (Automatic)  
 Pressure Relaxation= (Automatic)  
 Heat Transfer with Energy Balance (with Constant Density)  
 Fluid Database: AFT Standard  
 Fluid: Water at 1 atm  
 Max Fluid Temperature Data= 212 deg. F  
 Min Fluid Temperature Data= 32 deg. F  
 Temperature= 0 deg. C  
 Density= 999.8884 kg/m<sup>3</sup>  
 Viscosity= 0.00177 kg/sec-m  
 Vapour Pressure= 0.00704 bar  
 Viscosity Model= Newtonian  
 Apply laminar and non-Newtonian correction to: Pipe Fittings & Losses, Junction K factors, Junction Special Losses, Junction Polynomials  
 Corrections applied to the following junctions: Branch, Reservoir, Assigned Flow, Assigned Pressure, Area Change, Bend, Tee or Wye, Spray Discharge, Relief Valve  
 Ambient Pressure (constant)= 10 bar  
 Gravitational Acceleration= 1 g  
 Turbulent Flow Above Reynolds Number= 4000  
 Laminar Flow Below Reynolds Number= 2300  
 Total Inflow= 153.5 kg/sec  
 Total Outflow= 153.5 kg/sec  
 Total Energy Inflow= 25,754 kW  
 Total Energy Outflow= 2,614 kW  
 Maximum Static Pressure is 409.8 bar at Pipe 4 Inlet  
 Minimum Static Pressure is 0.9677 bar at Pipe 5 Outlet  
 Maximum Static Temperature is 40.00 deg. C at Junction 5 Inlet  
 Minimum Static Temperature is 4.000 deg. C at Junction 3 Inlet

Table II: Pressure and flow Rate for water case

Jct	Name	P Static In (bar)	P Static Out (bar)	P Staq. In (bar)	P Staq. Out (bar)	Vol. Flow Rate Thru Jct (m <sup>3</sup> /hr)	Mass Flow Rate Thru Jct (kg/sec)	Loss Factor (K)
1	Assigned Pressure	586.0	586.0	586.0	586.0	500.4	138.9	0
3	Branch	529.8	529.8	529.9	529.9	500.4	138.9	0
4	Branch	305.4	305.4	305.5	305.5	500.0	138.9	0
5	Assigned Flow	279.6	279.6	279.7	279.7	500.0	138.9	0
6	Branch	281.9	281.9	281.9	281.9	500.0	138.9	0

## II. Multi-Phase Flow Case

### II.1 Input data multi-phase flow case:

Pressure/Head Tolerance= 0.0001 relative change

Flow Rate Tolerance= 0.0001 relative change

Temperature Tolerance= 0.0001 relative change

Flow Relaxation= (Automatic)

Pressure Relaxation= (Automatic)

Heat Transfer with Energy Balance

Fluid Database: AFT Standard

Fluid: Benzene (liquid)

Max Fluid Temperature Data= 562.1 deg. K

Min Fluid Temperature Data= 278.69 deg. K

Default Temperature= 10 deg. C

Default Density= 885.0751 kg/m<sup>3</sup>

Default Viscosity= 0.00074794 kg/sec-m

Default Vapour Pressure= 0.06034 bar

Viscosity Model= Newtonian

Apply laminar and non-Newtonian correction to: Pipe Fittings & Losses, Junction K factors, Junction Special Losses, Junction Polynomials

Corrections applied to the following junctions: Branch, Reservoir, Assigned Flow, Assigned Pressure, Area Change, Bend, Tee or

Wye, Spray Discharge, Relief Valve

Ambient Pressure (constant)= 10 bar

Gravitational Acceleration= 1 g

Turbulent Flow Above Reynolds Number= 4000

Laminar Flow Below Reynolds Number= 2300

Table III: Pipes lengths/ sizes

Pipe	Name	Pipe Defined	Length	Length Units	Hydraulic Diameter	Hydraulic Diam. Units	Friction Data Set	Roughness	Roughness Units	Losses (K)	Initial Flow
1	Pipe	Yes	30	km	25.4508	cm	Standard	0.004572	cm	0	
2	Pipe	Yes	100	km	25.4508	cm	Standard	0.004572	cm	0	
3	Pipe	Yes	10	km	25.4508	cm	Standard	0.004572	cm	0	
4	Pipe	Yes	1	km	25.4508	cm	Standard	0.004572	cm	0	
Pipe	Initial Flow Units	Junctions (Up,Down)	Geometry		Material	Size	Type	Special Condition			
1		1, 3	Cylindrical Pipe		Steel - ANSI	10 inch	STD (s chedule 40)	None			
2		3, 4	Cylindrical Pipe		Steel - ANSI	10 inch	STD (s chedule 40)	None			
3		4, 6	Cylindrical Pipe		Steel - ANSI	10 inch	STD (s chedule 40)	None			
4		6, 5	Cylindrical Pipe		Steel - ANSI	10 inch	STD (s chedule 40)	None			

## II.2 Output data multi-phase flow case:

### Model Reference Information

Execution Time= 0.06 seconds  
 Total Number Of Head/Pressure Iterations= 0  
 Total Number Of Flow Iterations= 4  
 Total Number Of Temperature Iterations= 5  
 Number Of Pipes= 4  
 Number Of Junctions= 5  
 Matrix Method= Gaussian Elimination With Pivoting  
 Pressure/Head Tolerance= 0.0001 relative change  
 Flow Rate Tolerance= 0.0001 relative change  
 Temperature Tolerance= 0.0001 relative change  
 Flow Relaxation= (Automatic)  
 Pressure Relaxation= (Automatic)  
 Heat Transfer with Energy Balance  
 Fluid Database: AFT Standard  
 Fluid: Benzene (liquid)  
 Max Fluid Temperature Data= 562.1 deg. K  
 Min Fluid Temperature Data= 278.69 deg. K  
 Default Temperature= 10 deg. C  
 Default Density= 885.0751 kg/m<sup>3</sup>  
 Default Viscosity= 0.00074794 kg/sec-m  
 Default Vapour Pressure= 0.06034 bar  
 Viscosity Model= Newtonian  
 Apply laminar and non-Newtonian correction to: Pipe Fittings & Losses, Junction K factors, Junction Special Losses, Junction Polynomials  
 Corrections applied to the following junctions: Branch, Reservoir, Assigned Flow, Assigned Pressure, Area Change, Bend, Tee or Wye, Spray Discharge, Relief Valve  
 Ambient Pressure (constant)= 10 bar  
 Gravitational Acceleration= 1 g  
 Turbulent Flow Above Reynolds Number= 4000  
 Laminar Flow Below Reynolds Number= 2300  
 Total Inflow= 148.2 kg/sec  
 Total Outflow= 148.2 kg/sec  
 Total Energy Inflow= 30,337 kW  
 Total Energy Outflow= 28,987 kW  
 Maximum Static Pressure is 409.8 bar at Pipe 4 Inlet  
 Minimum Static Pressure is 0.9655 bar at Pipe 5 Outlet  
 Maximum Static Temperature is 30.00 deg. C at Junction 7 Inlet  
 Minimum Static Temperature is 4.000 deg. C at Junction 3 Inlet

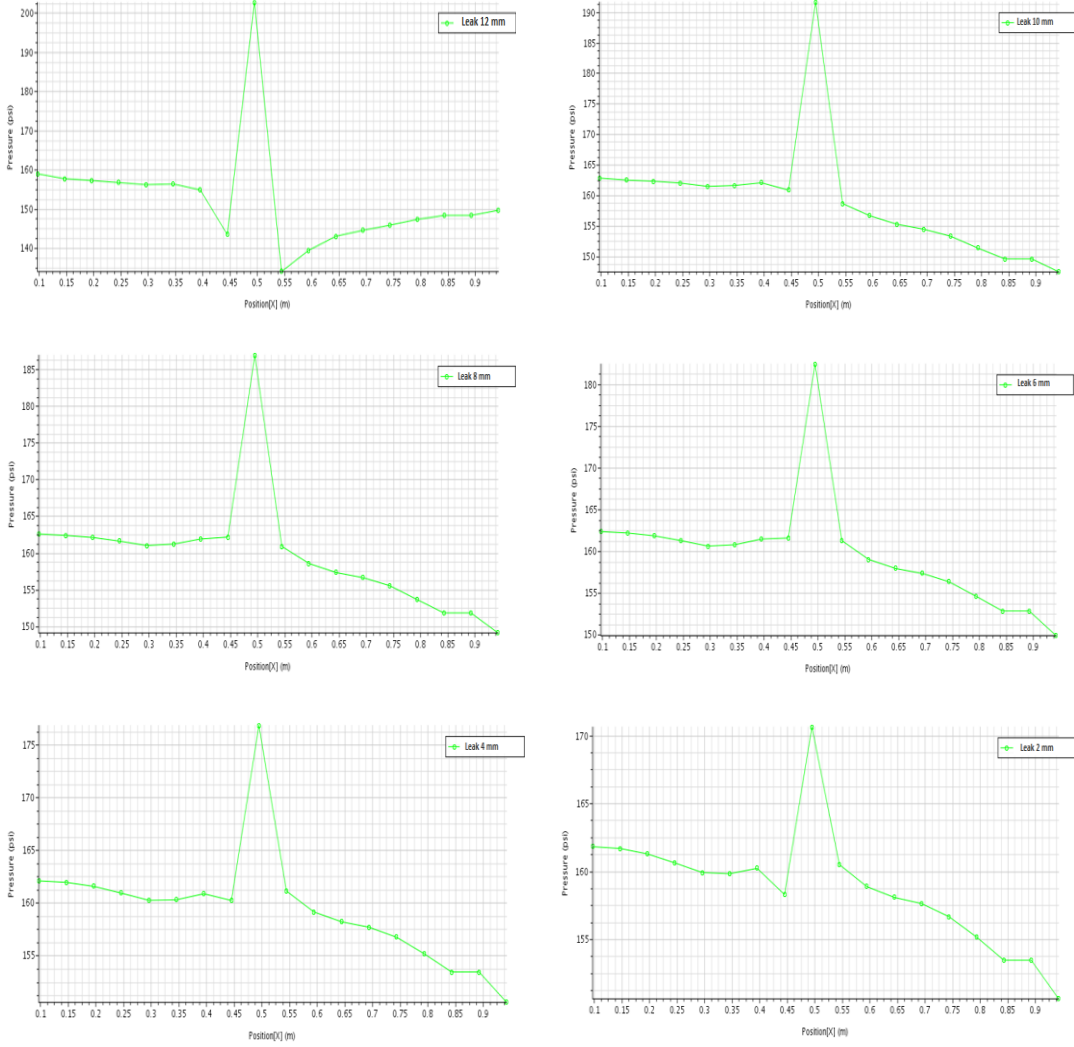
Table IV: Pressure and flow Rate for Benzene case

Jct	Name	P Static In (bar)	P Static Out (bar)	P Stag. In (bar)	P Stag. Out (bar)	Vol. Flow Rate Thru Jct (m <sup>3</sup> /hr)	Mass Flow Rate Thru Jct (kg/sec)	Loss Factor (K)
3	Branch	206.722	206.722	206.770	206.770	600.5	148.2	0.00000
5	Assigned Pressure	409.848	409.848	409.896	409.896	602.7	148.2	0.01000
6	Branch	409.303	409.303	409.351	409.351	602.7	148.2	0.00000
7	Reservoir	1.013	1.013	1.013	1.013	600.5	148.2	0.00000
8	Branch	68.607	68.607	68.655	68.655	600.5	148.2	0.00000

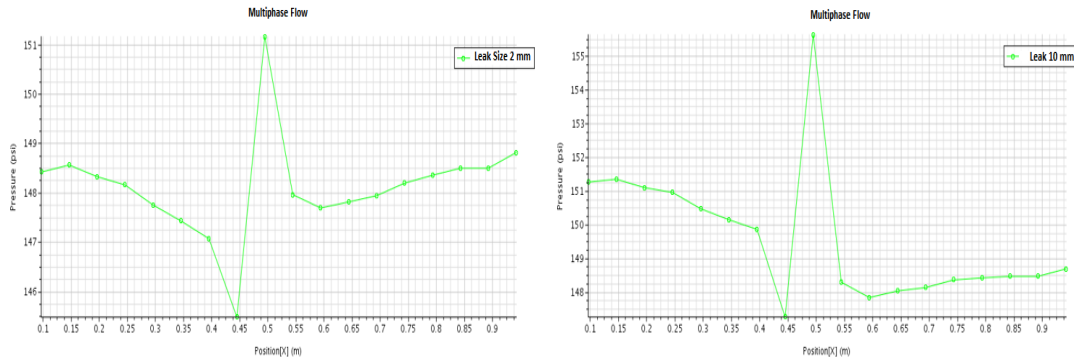
# Appendix B: CFD Model's Output Data

## I. Pressure Profile

### I.1 Pressure profile at different leak sizes for Single-phase flow case:

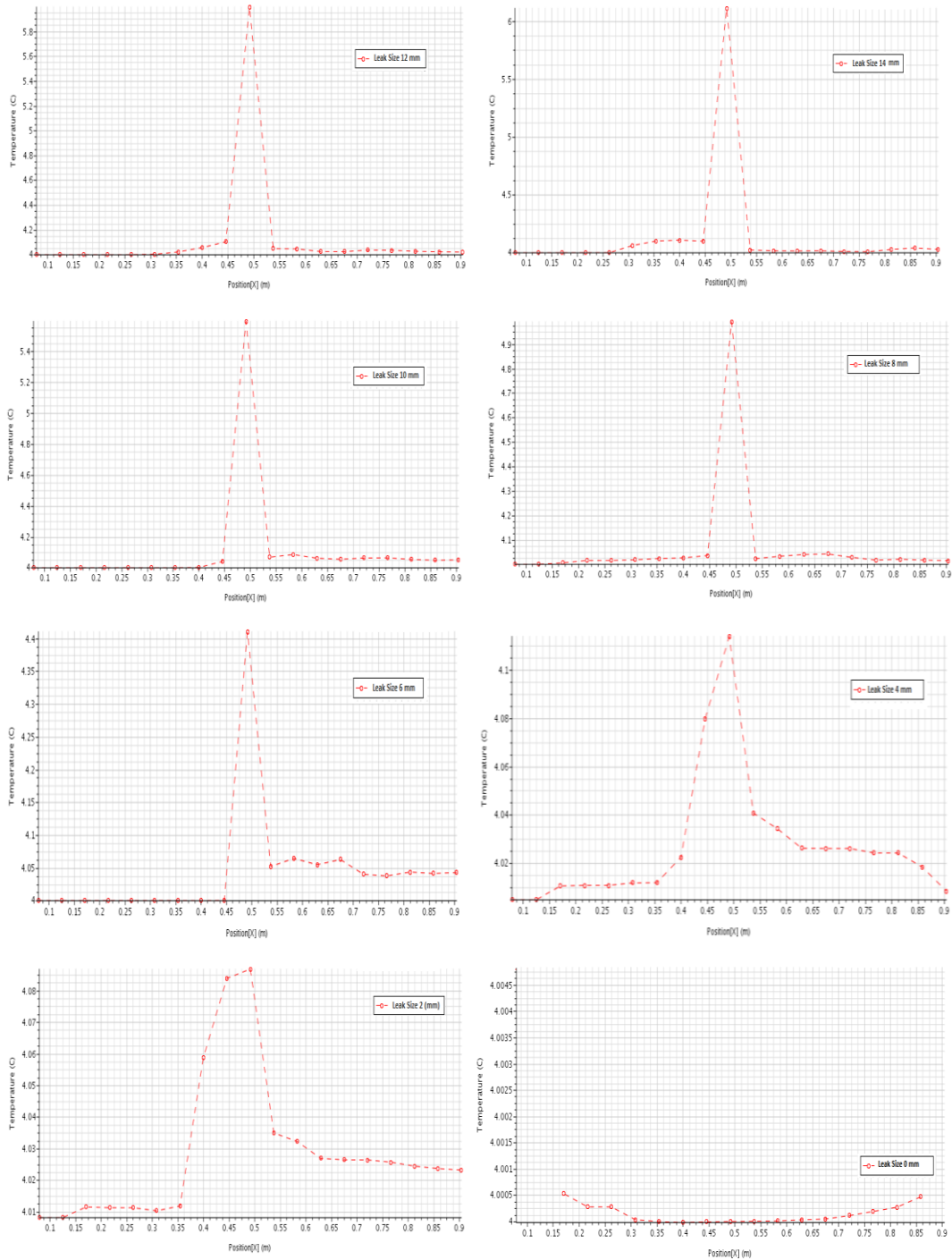


### I.2 Pressure profile at different leak sizes for Multi-phase flow case:

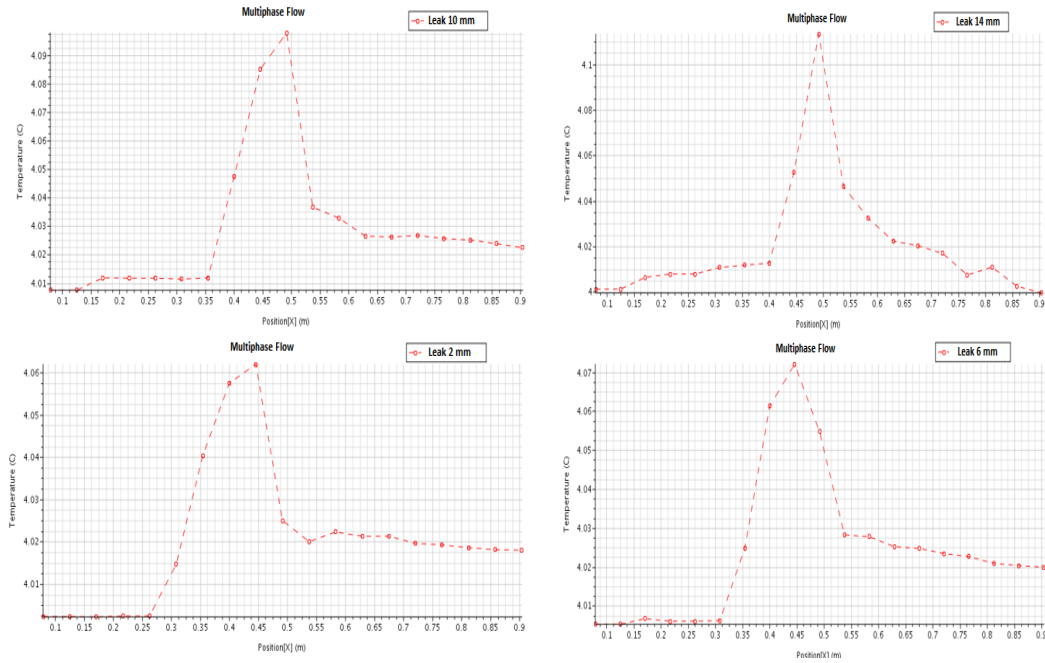


## II. Temperature Profile

### II.1 Temperature profile at different leak sizes for Single-phase flow case:

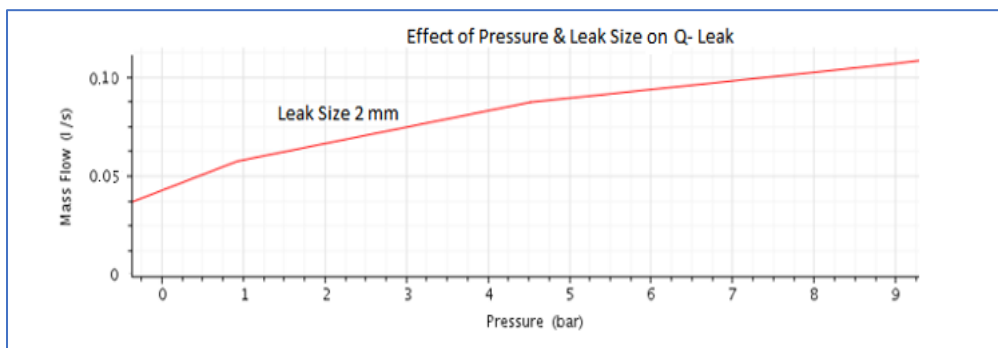
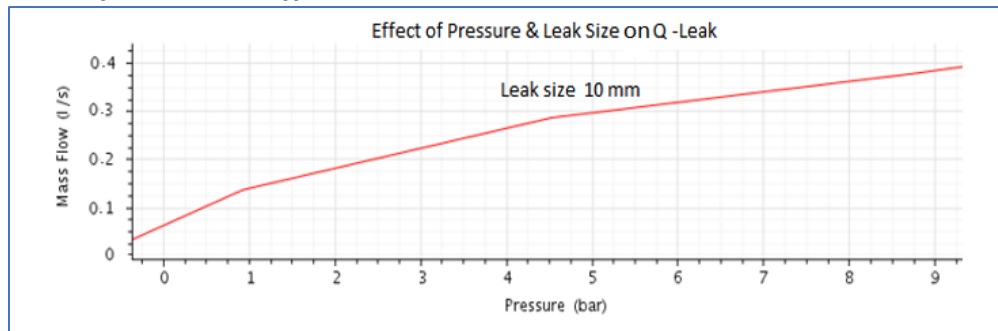


## II.2 Temperature profile for multi-phase flow case

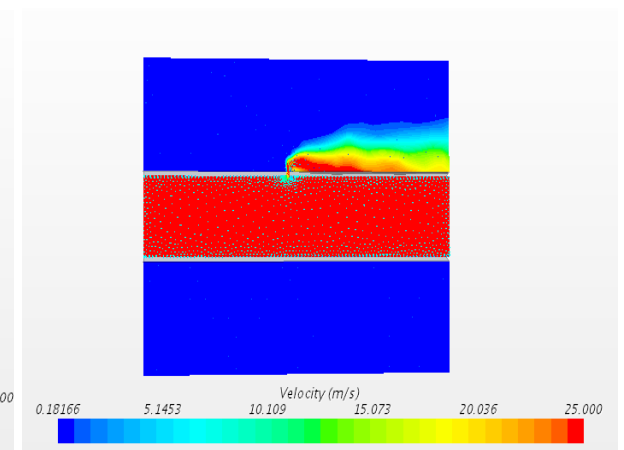
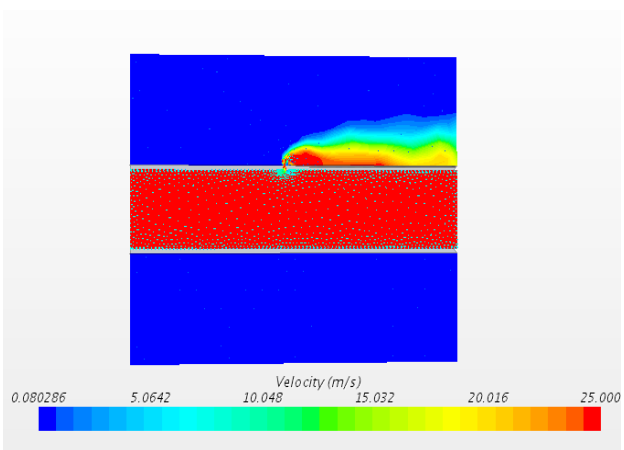
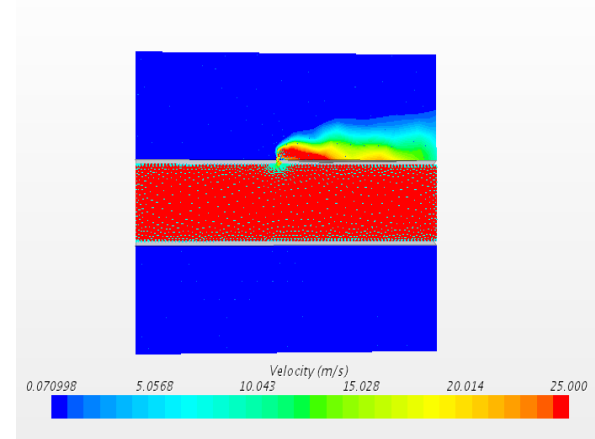
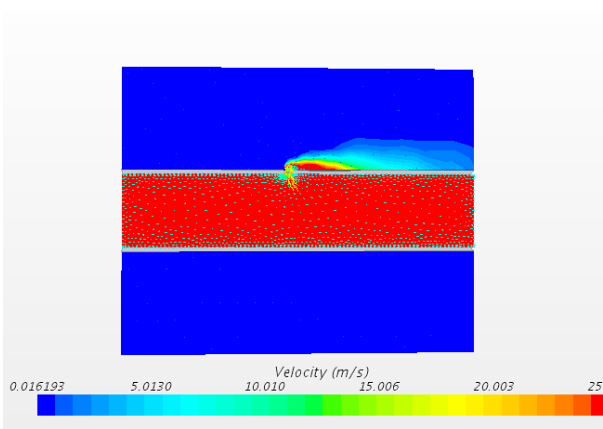
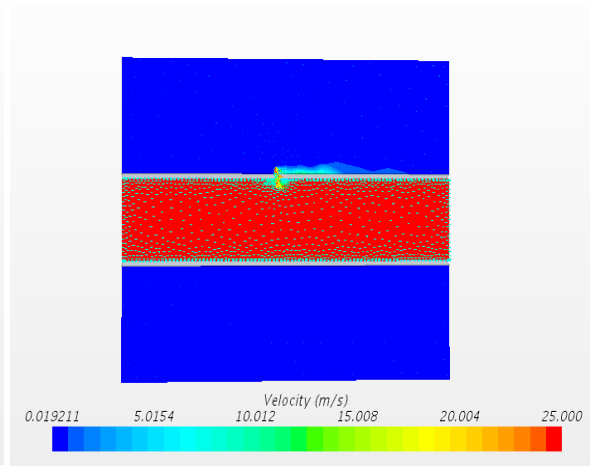
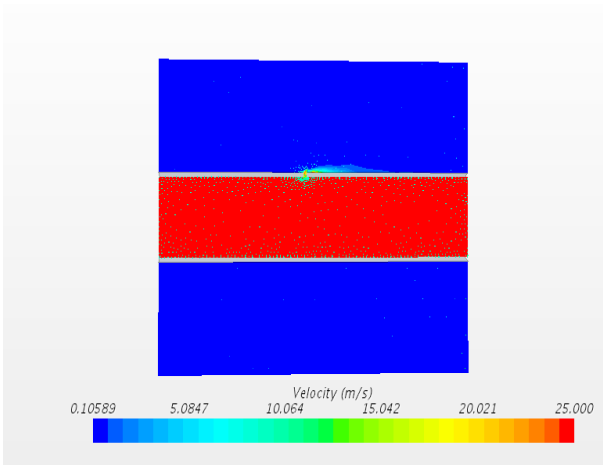


## III. Mass flow rate and velocity profiles

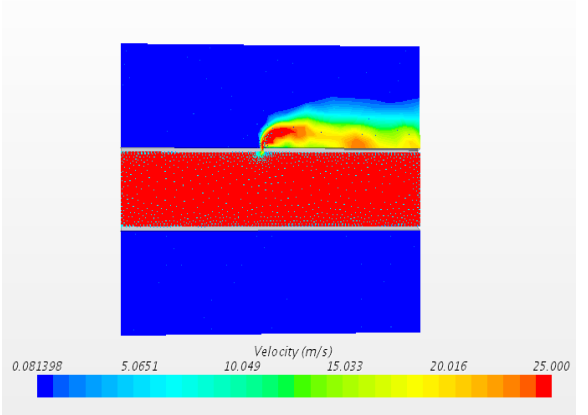
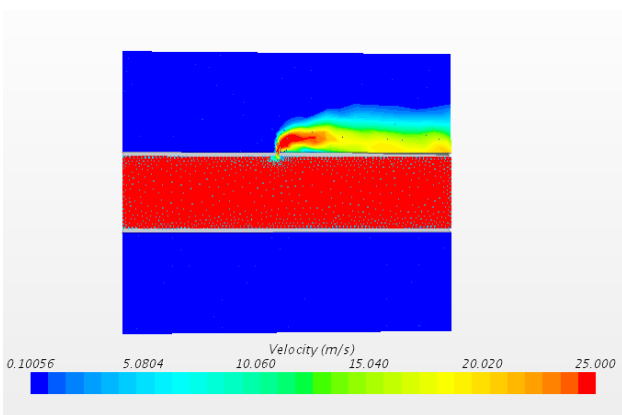
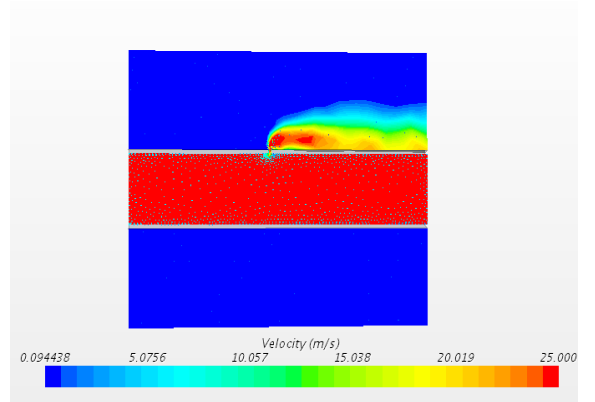
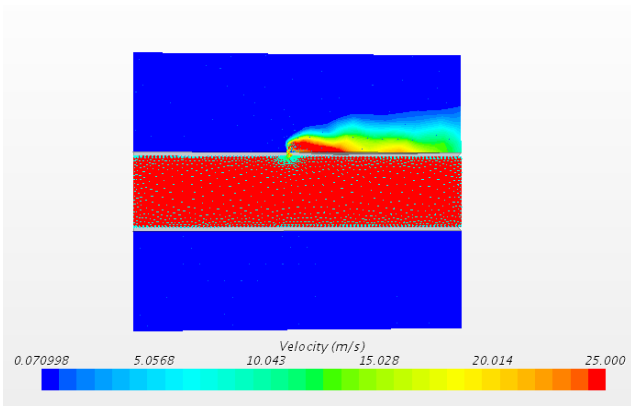
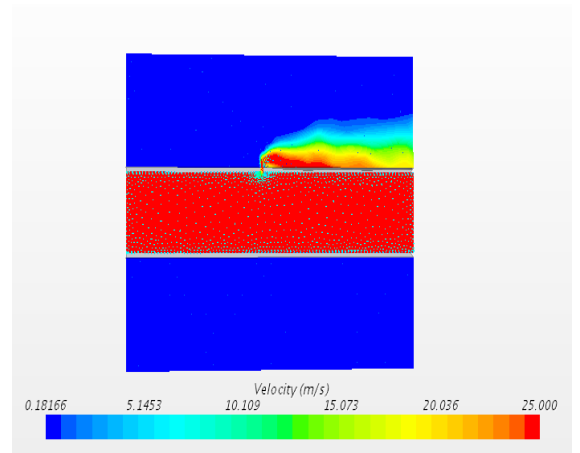
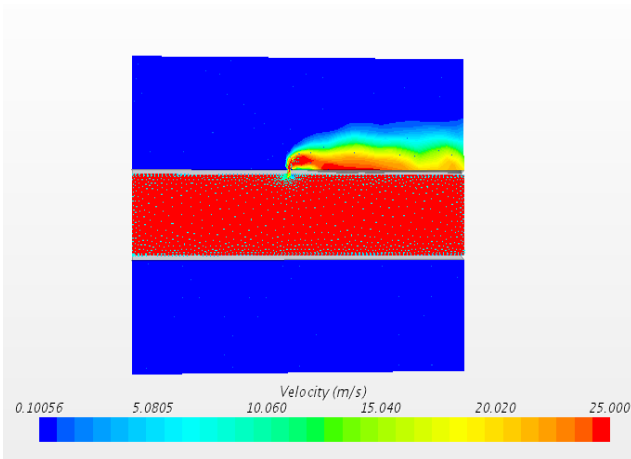
### III.1 Mass flow rate at different leak sizes



### III.1 3D Condensate velocity profile Vs time



### III.1 Cont. 3D Condensate velocity profile Vs time



### III.1 Condensate pressure profile Vs Time

